Ab Initio Calculations on Al_2N_4 and AlN_n ($n = 4$ to 7): Potential Precursors of High Energy Density Materials

Edmond P. F. Lee,*,† John M. Dyke,*,† and Rob P. Claridge‡

Department of Chemistry, Southampton University, Highfield, Southampton SO17 1BJ, United Kingdom, and Building R47, QinetiQ, Fort Halstead, Sevenoaks, Kent, TN14 7BP, United Kingdom

Received: April 25, 2002; In Final Form: June 24, 2002

Geometry optimization and harmonic vibrational frequency calculations have been carried out on various structures and low-lying, high- and low-spin electronic states of Al_2N_4 and AlN_n clusters, where $n = 4$ to 7, at the B3LYP, MP2, and QCISD levels. The aim of these calculations was to search for states/structures that may be suitable candidates as precursors of high energy density materials. Well-bound charge-transfer states/structures with activated NN bonds were obtained. The exothermicities of the decomposition reactions of these states/structures to N_2 molecules were computed at up to the RCCSD(T)/aug-cc-pVQZ(no g) level of theory. The most exothermic decomposition reaction considered is AlN_6 C_s Al·NN_2N_2N (N_6 ring), $^4A''$, $(a')^1(a')^1(a'')^1 \rightarrow Al + 3N_2$. The calculated $\Delta H^{298\,K}$ is −226 kcal/mol, giving an energy release of over 75 kcal/mol per N_2 molecule. We conclude that AlN_n systems are potential precursors of high energy density materials. In addition, the HOMOs of these states/structures have been examined in order to understand the stability of these states/structures. The ability of aluminum to introduce various degrees of covalency and ionicity to such clusters, which will stabilize the polynitrogen system, has been discussed.

Introduction

Polynitrogen species, N_n, have been studied extensively and suggested by computational chemists to be potential candidates for high energy density materials (HEDM) for nearly 20 years. (For recent works on N_n, see for examples refs 1−14 ; see references therein for earlier works.) However, the instability of these species, the low barrier to dissociation in particular (for examples, refs 1, 5, 7, and 15−19), appears to be a major hindrance for these molecules to have real applications. Nevertheless, the recent experimental successes of the research group of Christe et al. in synthesizing and characterizing two N_5^+-containing salts[3,20] have strengthened the theoretical prediction of polynitrogen species being potential candidates for HEDM. These experimental advances also have turned the attention of quantum chemists to cationic, anionic, and excited states of polynitrogen species (for examples, see refs 5, 8, 14, and 20−26).

In the search for potential candidates of HEDM, one faces an apparent dilemma. A suitable polynitrogen species should ideally have a large exothermicity upon dissociation to N_2 molecules, but at the same time, it should also have an appropriately high energy barrier to dissociation so that it can be stored safely before use (for examples, see refs 1,7,15,16,-18, and 19). To find a polynitrogen species that possesses these apparently contradictory properties of being highly energetic but also reasonably stable, some fundamental concepts of stability, for example, the potential energy hypersurfaces and bonding/antibonding interactions in a N_n species, need to be considered. In addition, one may need also to consider novel molecular systems, for example, a N_n system being stabilized by a metal center (M). In this connection, the metal atom may be viewed as a catalyst in the dissociation process of MN_n to $M + N_n$, which has an appropriately high energy barrier, followed by a low energy-barrier dissociation of N_n to $(^n/_2)N_2$. Recently, we reported an extensive ab initio and spectral simulation study[27] on the low-lying electronic states of GaN_2 in relation to the interpretation of its observed LIF spectra.[28] In the search for a suitable candidate for the upper state of the LIF band observed at 37 633 cm^{-1}, a number of linear and T-shaped charge-transfer quartet states, namely, $^4\Sigma^-$, 1^4B_1, 2^4B_2, and 1^4A_2, of GaN_2 were investigated for the first time. The computed molecular wave functions of these well-bound quartet states of GaN_2 show significant orbital mixing and electrostatic interaction between Ga and N_2, which lead to short computed GaN bond lengths and reasonably large intermolecular vibrational frequencies. At the same time, the computed NN bond lengths are significantly lengthened, whereas the NN stretching frequencies decrease, in comparison with those of isolated N_2, suggesting significant activation of N_2 in the complex. It was pointed out in ref 27 that in considering metal−dinitrogen interaction and N_2 activation by a metal center, attention had been focused mainly on transition metals.[29] However, ref 27 shows that a p-block semiconductor metal is able to have significant interaction with a dinitrogen molecule in a number of low-lying quartet states. In addition, considering the HOMOs and LUMOs of Ga and N_2, stabilization in these charge-transfer quartet states of GaN_2 can be rationalized as arising from the excitation of an electron from the Ga 4s localized HOMO to an N_2 localized antibonding LUMO. On the one hand, this excitation leads to charge transfer from Ga to N_2; on the other hand, there can be bonding interaction between Ga 4p (of the appropriate orientation) and the original N_2 localized antibonding LUMO, which would stabilize the system. The stability of these low-lying quartet states of GaN_2 is a result of delocalization of molecular orbitals (covalent bonding) and electrostatic attraction between the partially charged $Ga^{\delta+}$ and $N_2^{\delta-}$ molecular frag-

* Corresponding authors. E-mail: jmdyke@soton.ac.uk.
† Southampton University.
‡ QinetiQ, Fort Halstead.

10.1021/jp021059q CCC: $22.00
Published on Web 08/15/2002

ments (ionic bonding). (Further details are given in ref 27.) Following the excitation schemes to obtain these low-lying charge-transfer quartet states of GaN_2, we postulated that the kind of orbital interaction considered in ref 27 may lead to possible application in obtaining stabilized MN_n systems, which may be used as precursors of HEDM. As an illustration, the LUMOs and HOMOs of a hypothetical MN_4 ring system, where M is a p-block metal with a ground-state open-shell s^2p^1 valence electronic configuration like Ga, were examined in detail in ref 27. On the basis of considerations of the molecular orbitals and electrostatic interaction in the low-lying charge-transfer quartet states of GaN_2, it was anticipated that, with the appropriate electronic configurations, some quartet states of this hypothetical MN_4 ring system should be reasonably stable with a significant energy-well depth. In the present study, we report the results of our extensive ab initio and density functional calculations on some "real" systems (in contrast to the hypothetical MN_4 system)—AlN_n, where $n = 4$ to 7, and Al_2N_4 clusters. The AlN_4 ring system has been studied in detail. The results obtained for some quartet states of AlN_4 ring structures were found to be exactly in accordance with those postulated in ref 27 for the hypothetical MN_4 ring system. In addition, calculated results, including computed exothermicities upon dissociation to N_2 molecules obtained from high-level ab initio calculations on various structures of AlN_n clusters, with n up to 7, suggest strongly that AlN_n systems may be potential candidates for precursors of HEDM.

From the theoretical and computational point of view, Al was chosen as the metal center to be considered in the present investigation because it is a p-block metal, valence isoelectronic with Ga, but it is lighter than Ga. In this connection, calculations involving Al are simpler and computationally less demanding than calculations on Ga. From the practical or experimental point of view, the availability and stability of Al make it an attractive candidate. In this connection, it should be mentioned that ScN_7 has been recently studied by ab initio and density functional methods and considered to be a possible high-energy molecule containing an $[\eta^7\text{-}N_7]^{3-}$ ligand.[30] In addition, some heavier transition metals (Ti, Zr, Hf, and Th) have also been considered to stabilize polynitrogen clusters in a very recent theoretical study.[31] However, from the practical viewpoint of being readily available and of low cost, Al appears to be superior to these heavier transition metals. Some metal cation−pentazole anion complexes, where the metals considered are Na, K, Mg, Ca, and Zn, have also been studied by ab initio and density functional methods very recently.[32] With these alkali (Na and K), alkaline earth (Mg and Ca), and group IIB (Zn) metals, it is expected that the metal−pentazole complexes would be predominantly ionic in nature and that electrostatic interaction would dominate. The polynitrogen moiety in these complexes would behave essentially as a counteranion. In contrast, with a p-block metal such as Al or Ga, the MN_n complexes exhibit various degrees of covalent and electrostatic interaction in some of their low-lying electronic states (see ref 27 and later text), thus allowing more flexibility in the stabilization of the polynitrogen moiety of the complex by the metal center.

Al_xN_y clusters have received considerable attention from computational chemists in the past because of the importance of aluminum nitride (solid and thin-film AlN) in various industrial applications (see refs 33 and 34 and references therein). Most previous studies on Al_xN_y clusters were conducted by density functional methods[33−38] except for those on some small clusters, which have been studied by high-level ab initio calculations.[39−43] Apart from AlN_2, which was studied here for the purpose of establishing the appropriate methodology and theoretical basis for the investigation of the larger clusters, calculations on Al_2N_4 and AlN_n clusters, with $n = 4$ to 7, are reported here for the first time.

Theoretical Considerations and Computational Details. The initial calculations were on AlN_2. There are two main purposes for carrying out a series of calculations on AlN_2. First, a series of QCISD/6-311+G(3df) and CCSD(T)/6-311+G(3df) geometry optimization and harmonic frequency calculations were carried out on the various low-lying doublet and quartet states of AlN_2. Both linear and T-shaped structures were considered. This is for the purpose of establishing that AlN_2 behaves as GaN_2, particularly with regard to the existence of some low-lying charge-transfer quartet states, which are expected to show significant interaction between Al and N_2, as for GaN_2 reported in ref 27 and discussed above. To our knowledge, the only ab initio study available on AlN_2 is the MP2 and QCISD(T) calculations by Chaban and Gordon.[43] It appears that only the lowest-lying linear doublet states, $^2\Pi$ and $^2\Sigma$, were considered, with the former being very weakly bound and the latter repulsive. However, our interest is in well-bound charge-transfer quartet states. Second, a series of basis set variation calculations were carried out on the $\tilde{X}^2\Pi$ state of AlN_2 at different levels of theory. The main purpose of these calculations is to choose the most suitable basis set to be used in the calculations of larger AlN_n clusters. This is necessary because for larger clusters it is impractical to employ a large basis set. At the same time, for the search of stable structures of the larger clusters, correlation methods with analytical derivatives of energy with respect to geometrical parameters would be required because geometry optimization and harmonic vibrational frequency calculations employing numerical derivatives would be computationally too expensive. This consideration has ruled out the use of higher-order correlation methods, such as the CCSD(T) method, for calculations of the larger clusters because of the unavailability of analytical derivatives at the CCSD(T) level. In this connection, this series of calculations on AlN_2 also serves to compare the performance of different correlation methods employed for this type of compound; as for AlN_2, it is still possible to employ a correlation method with numerical derivatives of energy. In summary, the initial calculations on AlN_2 were made to establish a sound theoretical basis and a reliable methodology for further calculations on larger Aln_n clusters.

On the basis of the results obtained from the extensive study of basis set variation on AlN_2 mentioned above, the augmented correlation-consistent polarized-valence double-ζ (aug-cc-pVDZ) basis set was chosen to be used in calculations on Al_2N_4 and all AlN_n clusters with n larger than 2. Some MP2 calculations employing the 6-311+G(3df) basis set were also carried out on some selected states/structures of Al_2N_4 and AlN_4 as a further check of basis set effects on larger clusters (see later text). Geometry optimization and harmonic vibrational frequency calculations were performed on Al_2N_4 and AlN_n, $n = 4$ to 7, employing the most popular density functional method, B3LYP, and also the ab initio methods of MP2 and QCISD. However, QCISD calculations were carried out only for Al_2N_4 and AlN_n, where $n \leq 5$, because analytical second derivatives are not available for the QCISD method. Numerical second derivative calculations on AlN_n, where n is larger than 5, become impracticably expensive with the QCISD method. Nevertheless, for Al_2N_4 and AlN_5, a number of selected states/structures were studied using the QCISD method as a check on the effects of higher-order electron correlation on the optimized geometrical

parameters and computed harmonic vibrational frequencies. All of the above geometry optimization and harmonic frequency calculations were performed using the Gaussian suite of programs.[44]

Relative electronic energies were calculated at a higher level of theory using the RCCSD(T) method[45] as implemented in the MOLPRO suite of programs,[46] which is known to be the most reliable single-configuration method for electron correlation. Large basis sets of up to aug-cc-pVQZ quality, with a total number of contracted Gaussian basis functions of over 300, were employed to yield reliable computed reaction energetics. Thermodynamic constants of the following decomposition reactions were evaluated within the harmonic oscillator−rigid rotor model.

$$Al_2N_4 \rightarrow 2Al + 2N_2$$

For even n, $AlN_n \rightarrow Al + (n/2)N_2$

For odd n, $AlN_n \rightarrow AlN + \{(n-1)/2\}N_2$ and

$$AlN_n \rightarrow Al + (n/2)N_2$$

Because of the limited computational resources available, some restrictions imposed in the present investigation are summarized as follows:

Species Considered: Al_2N_4 and AlN_n, $n = 4$ to 7.

Structures Considered: (1) AlN_4: A large number of structures, including the linear, T-shaped, rectangular N_4 with Al on top, planar five-membered rings (Al as part of the ring) and near-tetrahedral N_4 structures with Al at a vertex, a side, or a face were considered;

(2) Al_2N_4: Rectangular N_4 structures, with the two Al atoms on opposite sides or above and below N_4;

(3) For AlN_n, where $n > 4$, only n-membered N_n ring and $(n + 1)$-membered ring (Al as part of the ring) structures were considered. For the n-membered N_n ring structure, Al is bonded either to a vertex or a side.

Electronic States Considered: (1) Low-lying singlet and triplet states for odd n, where n is the number of N atoms in the AlN_n system;

(2) Low-lying doublet and quartet states for even n;

(3) Low-lying singlet and triplet states for Al_2N_4.

The general strategy used in the search for stable states/structures is as follows. The B3LYP method was employed first for a general survey of different states/structures. This was followed by MP2 calculations on the relevant optimized states/structures obtained by the B3LYP method. Some relevant electronic states/structures, which had not been obtained from the B3LYP calculations, were also considered at the MP2 level. Selected states/structures obtained at the MP2 levels were then considered at the QCISD level. Finally, the electronic energy changes of some selected representative dissociation reactions were calculated at the RCCSD(T) level.

Results and Discussion

AlN_2. The results obtained for various states/structures of AlN_2 are summarized in Tables 1 to 3. On the basis of the results shown in Table 1, the aug-cc-pVDZ basis set was chosen for further calculations on larger AlN_n clusters as a compromise between economy and reliability. The 6-311+G(3df) basis set may be considered as a better choice than the aug-cc-pVDZ basis set from the viewpoint of accuracy of the results, but it will be too expensive for calculations of most of the larger clusters. Nevertheless, as mentioned above, some MP2/6-311+G(3df) geometry optimization and harmonic vibrational frequency calculations were carried out on selected states/structures of AlN_4 and Al_2N_4. The results obtained using the 6-311+G(3df) and aug-cc-pVDZ basis sets at the MP2 level of calculation are essentially identical for the AlN_4 states/structures considered, suggesting that the aug-cc-pVDZ basis set is reasonably adequate for AlN_n clusters. The MP2/6-311+G(3df) results on the Al_2N_4 states/structures will be discussed later.

TABLE 1: Optimized Geometrical Parameters and Computed Harmonic Vibrational Frequencies (cm^{-1}) of the $\tilde{X}^2\Pi$ State of AlN_2 Obtained at Different Levels of Calculation[a]

method	AlN/Å	NN/Å	$\omega_1(\sigma)$	$\omega_2(\sigma)$	$\omega_3(\pi)$
B3LYP/6-311+G(3df)	1.994	1.131	1950	306	233; 306
MP2/6-31+G(2d)	3.511	1.122	2249	48	56; 61
MP2/aug-cc-pVDZ	3.471	1.130	2607	52	41; 42
MP2/6-311+G(2d)	3.500	1.114	2196	47	52; 58
MP2/6-311+G(3df)	3.359	1.113	2231	55	57; 58
QCISD/6-311+G(3df)	3.541	1.097	2405	43	54; 54
CCSD(T)/6-311+G(3df)	3.395	1.103	2343	50	58; 59
MP2/aug-cc-pVTZ[b]	3.39	1.114		52	
MP2(full)/aug-cc-pCVTZ[b]	3.35	1.110			
QCISD(T)/aug-cc-pVTZ[b]	3.43	1.104		44	
QCISD(T,full)/aug-cc-pCVTZ[b]	3.40	1.101			

[a] The MP2 and QCISD calculations are with frozen cores, except otherwise stated. [b] From Chaban and Gordon.[43]

Comparing the results in Tables 2 and 3 with those of the doublet and quartet states of GaN_2 given in refs 47 and 27, respectively, it is clear that AlN_2 behaves essentially in the same way as GaN_2 does in the low-lying doublet and quartet states. Specific to the purpose of the present investigation, there are well-bound charge-transfer quartet states of AlN_2, just as for GaN_2. On the basis of the results of AlN_2 obtained here and by comparison with those of GaN_2 reported in ref 27, it is anticipated that for the AlN_4 ring system some well-bound charge-transfer quartet states with the appropriate electronic configurations should exist, as postulated in ref 27 for a hypothetical MN_4 ring system.

First, regarding the performance of the various correlation methods used in the calculation of AlN_2, some comments should be made on the reliability of the density functional method, B3LYP, for the kind of molecular systems studied here. On the basis of the results of AlN_2 obtained in the present study (see footnotes a and b of Table 3) and those of GaN_2 reported previously in refs 27 and 47, the B3LYP method gives essentially identical results to the ab initio results for almost all well-bound charge-transfer states. However, it can be seen that the B3LYP method tends to predict stable states/structures for states/structures that are predicted to be weakly bound by ab initio methods. (For example, the $\tilde{X}^2\Pi$ state of AlN_2 in Table 1; see also ref 27.) Such findings also occur for larger clusters of AlN_n, which will be discussed below. In addition, for Al_2N_4, most of the B3LYP results were found to be different from the MP2 and QCISD results (see later text). Our view at present is that ab initio results should be more reliable than density functional results, when they differ. Bearing this in mind and on the basis of the results of AlN_n and Al_2N_4 obtained here, all calculated results reported previously for Al_xN_y clusters, obtained only by density functional methods mentioned in the Introduction, should be viewed with caution. One particular concern relevant to the present study is that states/structures predicted to be well bound by density functional calculations can turn out to be very weakly bound by ab initio calculations. Our conclusion here is that density functional calculations should always be checked by ab initio calculations. At least qualitative agreement between density functional and ab initio results should be obtained before the former can be concluded to be reliable.

TABLE 2: Optimized Geometrical Parameters, Computed Harmonic Vibrational Frequencies (cm^{-1}), and Relative Electronic Energies, E_{rel}[a], of the Lowest-Lying T-Shaped Doublet States and Linear and T-Shaped Quartet States of Al·N_2 at the QCISD/6-311+G(3df) Level of Calculation

state	configuration	AlN/Å	NN/Å	NAlN/deg	$\omega_1(a_1)$	$\omega_2(a_1)$	$\omega_3(b_2)$	E_{rel}/eV
$^2A_1$	$(a_1)^1$	5.2254	1.0975	12.1	2404.6	17.8	24.1	0.0254
$^2B_1$	$(b_1)^1$	4.3192	1.0976	14.6	2403.7	23.9	36.4i	0.3664
$^2B_2$	$(b_2)^1$	4.3414	1.0978	14.5	2402.3	20.9	35.6i	0.0270
$^4\Sigma^-$ [b]	$(\sigma)^1(\pi)^2$	1.8246	1.1340		1901.4	524.8	359.5	2.2307
$^4B_1$	$(a_1)^1(b_2)^1(a_2)^1$	1.8324	1.3233	42.3	1201.1	694.2	649.2i	3.4436
$^4B_2$	$(a_1)^1(a_2)^1(b_1)^1$	2.0415	1.2012	34.2	1817.0	509.2	228.3i	4.6398
$^4A_2$	$(a_1)^1(b_2)^1(b_1)^1$	2.0353	1.1705	33.4	1834.2	469.9	260.6	2.9879

[a] With respect to the linear $\tilde{X}^2\Pi$ state. [b] Linear AlN_2; the symmetries of the vibrational frequencies are σ, σ and π respectively.

TABLE 3: Optimized Geometrical Parameters, Computed Harmonic Vibrational Frequencies (cm^{-1}), Relative Energies (E_e), Charge (q), and Spin (s) Densities of the Ground State and Some Quartet Charge-Transfer States of AlN_2 at the CCSD(T)/6-311+G(3df) Level of Calculation

states	$\tilde{X}^2\Pi$	$^4\Sigma^-$	$^4A_2$	$^4B_1$	$^4B_2$
AlN/Å	3.395	1.815[a]	2.046[b]	1.837	2.044
NN/Å	1.103	1.142	1.176	1.330	1.209
ω_1(NN)	2343	1858	1783	1176	*c*
$\omega_2(\sigma$ or $a_1)$	50	549	453	679	
$\omega_3(\pi$ or $b_2)$	58; 59	359	318	330	
E_e/kcal mol^{-1}	0.0	50.2	67.5	77.8	106.2
Q_{Al}	−0.057	0.091	0.420	0.802	0.517
Q_N	−0.127; 0.183	0.282; −0.373	−0.210	−0.401	−0.259
S_{Al}	0.998	2.752	2.262	0.855	1.983
S_N	−0.010; 0.013	−0.801; 1.237	0.399	1.072	0.509

[a] At the B3LYP/6-311+G(3df) level of calculation, the optimized geometrical parameters for the $^4\Sigma^-$ state are AlN = 1.780 and NN = 1.146 Å, the computed harmonic vibrational frequencies are 1826, 605, and 359 cm^{-1}, and the relative E_e is 49.7 kcal/mol above the $\tilde{X}^2\Pi$ state. [b] At the B3LYP/6-311+G(3df) level of calculation, the optimized geometrical parameters for the $^4A_2$ state are AlN = 2.043 and NN = 1.165 Å, the computed harmonic vibrational frequencies are 1857, 456 and 140i cm^{-1}, and the relative E_e is 70.7 kcal/mol above the $\tilde{X}^2\Pi$ state. [c] Unphysical values; see text.

Regarding the different ab initio methods employed here for the calculations of AlN_2, in general, it can be concluded that they give consistently the same qualitative result that the $\tilde{X}^2\Pi$ state is a weakly bound state. Specifically, the MP2 results are very similar to the CCSD(T) and QCISD(T) results with the same basis set (Table 1). The QCISD method gives a slightly longer AlN bond length and smaller intermolecular vibrational frequencies. It appears that triple excitations are important for this kind of weakly bound species. Nevertheless, for the stable charge-transfer quartet states, the QCISD and CCSD(T) results are very consistent, suggesting that the demand on electron correlation is only modest for these stable states/structures. Stability in these charge-transfer quartet states appears to have come mainly from the Hartree−Fock wave functions, with minor contributions from electron correlation. In conclusion, for calculations on larger AlN_n clusters, B3LYP results should be viewed with caution, but the MP2 results should be reasonably reliable. In the following discussion, we focus on states/structures that have consistent ab initio and density functional results, particularly for the larger clusters.

AlN_4. The computed results of the various states/structures of AlN_4 obtained at different levels of calculation are summarized in Tables 4 to 9. Only the low computed harmonic vibrational frequencies are given in these Tables to show whether the stationary points obtained are minima and/or to show qualitatively the expected well depth (small computed vibrational frequencies suggest a shallow minimum). Some of the representative structures obtained are shown in Figure 1. Although obtaining the ground-state structure of AlN_4 is not the main purpose of the present investigation, both the B3LYP and MP2 results suggest that a $^2B_1$ state with a C_{2v} V-shaped $(N_2)Al(N_2)$ structure is likely to be the lowest state/structure of AlN_4. The computed AlN bond length of greater than 3.4 Å and the low vibrational frequency of 24 cm^{-1} obtained for this structure at the MP2 level (Table 5) indicate that it is a very weakly bound state. However, the optimized B3LYP geometry and computed harmonic vibrational frequencies (Table 4) suggest significantly stronger bonding than that from the MP2 calculations. As mentioned above, the B3LYP method tends to give a more stable state/structure for a state/structure that is weakly bound by ab initio methods. At the QCISD level, geometry optimization for this state did not converge even after 25 points (Table 7). On the basis of what has been discussed above on AlN_2, the neglect of triple excitations in the QCISD calculation is possibly the cause of the failure of convergence in the geometry optimization of this state/structure. Nevertheless, the last geometry and the computed charge and spin densities obtained in the QCISD calculations are very similar to those obtained at the MP2 level and also suggest a very weakly bound state/structure. Our conclusion here follows what has been discussed above, that the B3LYP results are probably unreliable for this state/structure. The lowest state/structure obtained at the QCISD level is the linear N_2·Al·N_2 $^2\Pi_u$ state (Table 8), which is only 0.66 kcal/mol above the V-shaped $^2B_1$ state/structure at the MP2/aug-cc-pVDZ level (Table 6). This linear $^2\Pi_u$ state has a long computed AlN bond length of over 3.5 Å and very low computed vibrational frequencies of ca. 10 cm^{-1} at the MP2 and QCISD levels of calculation, suggesting a very weakly bound state (Tables 6 and 8). It seems clear that the lowest state/structure of AlN_4 is almost certainly a weakly bound doublet state, though whether it has a V-shaped or linear structure would require further investigation.

In general, most of the doublet states of AlN_4 considered here are either saddle points with one or more computed imaginary vibrational frequencies or very weakly bound minima with long intermolecular computed bond lengths and low vibrational frequencies. The only doublet state that may be well bound is the $^2A_1$ state of the AlN_4 ring structure, with a computed AlN bond length of 2.291 Å and the lowest computed vibrational frequency of 155.5 cm^{-1} at the MP2 level (Table 5). However, at the B3LYP level, it is a first-order saddle point (Table 4), and at the QCISD level (Table 1), it was unoptimized after 25 points from the MP2 optimized geometry. The last geometry in the QCISD geometry optimization has a long AlN bond length of 4.7 Å and a long N···N intermolecular bond length of 5.2 Å (Table 1), suggesting that the system is falling apart. It is unclear whether inclusion of triple excitations in the correlation calculation would stabilize this state/structure. The results obtained here for the $^2A_1$ ring structure show that higher-level calculations than have been employed are required to obtain unambiguous results for this electronic state.

TABLE 4: Optimized Geometrical Parameters (Å), Computed Harmonic Vibrational Frequencies (cm^{-1}), Total Electronic Energies (E_e in hartrees), Charge (q), and Spin (s) Densities of Various Structures and Electronic States of AlN_4 at the B3LYP/aug-cc-pVDZ Level of Calculation

structure	state	configuration/E_e	optimized geometry	frequency	q_{Al}; s_{Al}
N_2·Al·N_2	$^2\Pi_u$	$(\pi_u)^1$	AlN = 2.001	136.7i(π_u); 91.5i(σ_u)	0.353; 1.227
		−461.37465	NN = 1.133		
N_2·Al···N_2	$^2\Pi$	$(\pi)^1$	AlN = 2.069; 5.422	7.0(σ); 10.3;10.9(π)	0.138; 0.539
		−461.47485	NN = 1.139; 1.104		
near-tetrahedral, side	$^2B_2$	$(b_2)^1$	AlN = 2.165	98.7i(b_2); 196.4(b_1)	0.348; 0.038
		−461.21186	NN = 1.469; 1.464		
rect-N_4, top	$^2B_1$	$(b_1)^1$	AlN = 5.924	16.2i(a_2); 12.1i(b_2)	0.004; 0.999
		−461.46920	NN = 1.104; 7.401		
rect-N_4, top	$^4B_2$	$(b_2)^1(b_1)^1(b_1)^1$	AlN = 2.492	382.3i(b_2); 349.4i(b_1)	0.478; 0.254
		−461.26634	NN = 1.216; 2.007		
N_2·Al·(N_2), T	$^4A_2$	$(a_1)^1(b_1)^1(b_2)^1$	AlN = 1.804; 5.334	21.4i(b_2); 8.0(a_1)	0.204; 2.415
		−461.39329	NN = 1.156; 1.104		
near-tetrahedral, face	$^4A_1$	$(e)^2(a_2)^1$	AlN = 2.098	233.0(e); 295.5(a_1)	0.539; −0.217
		−461.20339	NN = 1.381; 2.244		
near-tetrahedral, side	$^4A_2$	$(a_1)^1(b_1)^1(b_2)$	AlN = 2.222	96.5(b_2); 196.8(b_1)	0.432; 0.170
		−461.22130	NN = 1.901; 1.447		
near-V[a]	$^2B_1$	$(b_1)^1$	AlN = 2.197	84.2(a_1); 128.1(b_2)	0.148; 0.520
		−461.47726	NN = 1.122; 2.671		
near-V[a]	$^4B_1$	$(a_1)^1(b_1)^1(a_1)^1$	AlN = 1.924	31.0(a_1); 138.9(a_2)	0.346; 2.065
		−461.39719	NN = 1.145; 3.284		
ring	$^2A_1$	$(a_1)^1$	AlN = 2.359	171.5i(b_2); 118.8(b_1)	0.326; 0.342
		−461.46370	NN = 1.133; 2.708		
ring	$^4B_2$	$(a_2)^1(b_1)^1(a_1)^1$	AlN = 1.956	371.9(b_1); 390.1(b_2)	0.595; 0.792
		−461.24317	NN = 1.399; 1.299		
ring	$^4A_2$	$(b_2)^1(b_1)^1(a_1)^1$	AlN = 2.132	172.5(b_1); 220.9(b_2)	0.414; 0.509
		−461.32682	NN = 1.237; 1.341		
N_2·Al·N_2	$^4\Sigma_u^-$	$(\sigma_g)^1(\pi_u)^1$	AlN = 2.017	11.7(π_u); 153.5(π_g)	0.315; 2.314
		−461.39651	NN = 1.128		

[a] The initial geometry has a ring structure.

TABLE 5: Optimized Geometrical Parameters (Å), Computed Harmonic Vibrational Frequencies (cm^{-1}), Total Electronic Energies (E_e in hartrees), Charge (q), and Spin (s) Densities of Various Electronic States of the Al·N_4 Ring Structure at the MP2/aug-cc-pVDZ Level of Calculation

state	configuration/E_e(au)	optimized geometry (Å)	frequency (cm^{-1})	q_{Al}; s_{Al}/q_N; s_N
$^2A_1$	$(a_1)^1$	Al = 2.291	155.5(b_1); 236.1(b_2)	0.461; 0.327
	−460.43859	NN = 1.137; 2.249		−0.123; −0.16
$^2B_2$	$(b_2)^1$	AlN = 1.841	447.8i(b_2); 351.4i(b_1)	1.021; −1.400
	−460.25205[a]	NN = 1.307; 1.311		−0.421; 1.336
$^2B_1$	$(b_1)^1$	AlN = 3.420	24.2(a_1); 37.1(b_2)	−0.046; 1.012
	−460.47237[b]	NN = 1.130; 3.263		−0.030; −0.050
$^4A_1$	$(a_2)^1(b_2)^1(b_1)^1$	AlN = 2.108	610.9(a_2); 894.9(a_1)	0.498; −0.134
	−460.17355	NN = 1.409; 1.279		−0.209; 1.606
$^4B_1$	$(a_2)^1(b_2)^1(a_1)^1$	AlN = 1.811	894.4(a_1); 966.3(b_2)	0.667; 0.237
	−460.17605	NN = 1.481; 1.248		−0.321; 1.467
$^4A_2$	$(b_2)^1(b_1)^1(a_1)^1$	AlN = 2.172	222.3(a_1); 330.2(b_2)	0.610; 0.152
	−460.26175	NN = 1.224; 1.408		−0.158; 1.488
$^4B_2$	$(a_2)^1(b_1)^1(a_1)^1$	AlN = 1.929	688.4i(b_1); 450.1(b_1)	1.092; 0.921
	−460.19456	NN = 1.405; 1.331		−0.475; 1.019

[a] Very large spin contamination ($\langle S^2 \rangle = 1.95$). [b] Optimized to a near-V-shaped structure.

In contrast to the doublet states, there are a large number of quartet states that appear to be reasonably strongly bound with short computed AlN bond lengths and reasonably large vibrational frequencies. First, the ring structures were considered. Four quartet states ($^4A_1$, $^4B_1$, $^4A_2$, and $^4B_2$; see Tables 4, 5, and 7) were studied. The electronic configurations of these excited quartet states were chosen according to the excitation schemes suggested in ref 27. Briefly, electrons were excited from antibonding combinations of N_2 bonding HOMOs ($7b_2$, $2b_1$, and $1a_2$) to bonding combinations of N_2 antibonding LUMOs ($11a_1$ and $3b_1$), which could be mixed with Al 3p orbitals of the appropriate orientations. The optimized geometrical parameters of these quartet states obtained at different levels of calculations are reasonably consistent, having short intermolecular AlN and long intramolecular NN bond lengths, as anticipated. The computed charge and spin densities obtained at the optimized geometries of these states suggest various degrees of covalent (noninteger spin densities) and electrostatic (nonzero charge on Al) interaction, exactly as hypothesized in our second paper[27] on GaN_2, based on consideration of molecular orbitals. Among the four quartet states studied, all real computed vibrational frequencies were obtained only for the $^4A_2$ state at all levels of calculation. Whereas the $^4B_2$ state is a true minimum at the B3LYP level of calculation, it is a first-order saddle point at the MP2 level. At the QCISD level, numerical second derivative calculations for three of the four quartet states of the ring structures that were considered faced QCISD iteration problems at geometries displaced from the optimized positions (Table 7; also see later text). Consequently, for these three states, it is uncertain whether they are true minima on the hypersurface at the QCISD level. In any case, the computed results on the $^4A_2$ state of AlN_4, which is the lowest quartet state studied, are very

TABLE 6: Optimized Geometrical Parameters (Å), Computed Harmonic Vibrational Frequencies (cm^{-1}), Total Electronic Energies (E_e in hartrees), Charge (q), and Spin (s) Densities of Various Electronic States of Other Structures of AlN_4 at the MP2/aug-cc-pVDZ Level of Calculation

structure/state	optimized geometry (Å)	frequency (cm^{-1})/E_e(hartrees)	q_{Al}; s_{Al}/q_N; s_N
C_{3v}, near-tetrahedral N_4,	AlN = 1.980	3408i(e); 359(a_1)	1.09; 1.30;
Al at face; $^4A_2$ $(a_1)^1(e)^2$	NN = 1.830; 1.582	−460.03019	−0.46; 0.01
C_{2v}, near-tetrahedral N_4, Al at side;	AlN = 3.130	37(b_1); 73(a_1)	−0.08; 1.02
$^4A_1$ $(b_2)^1(a_1)^1(b_2)^1$	NN = 1.588; 1.445	−460.09690	0.02; −0.15
C_{3v} N(N_3)·Al, near-tetrahedral N_4	AlN = 2.167	364(a); 544(e)	0.64;−0.01;
with Al at face[a]; $^4A_1$ $(e)^2(a_2)^1$	NN = 1.344; 2.294	−460.14386	−0.32; 0.31
C_{2v}, near-tetrahedral N_4, Al at side;	AlN = 2.211	271(b_1); 347(a_1)	0.60; 0.04
$^4A_2$ $(b_1)^1(b_2)^1(a_1)^1$	NN = 1.912; 1.457	−460.17819	−0.17; 0.49
C_{2v}, near-tetrahedral N_4, Al at side;	AlN = 2.157	136(b_2); 247(b_1)	0.545; 0.009
$^2B_2$ $(b_2)^1$	NN = 1.484; 1.504; 2.016	−460.19932	−0.098; −0.174
C_{2v}, rectangular N_4, Al on top;	AlN = 2.442	183(b_1); 301(a_1)	0.550; 0.189
$^4B_2$ $(b_2)^1(b_1)^1(b_1)^1$	NN = 1.257; 2.009	−460.25851	−0.138; 0.703
C_{2v}, T-shaped, NN·Al·N_2;	AlN = 2.602; 2.325	72(b_2); 86(b_1)	0.183; 2.756
$^4A_2$ $(a_1)^1(b_2)^1(b_1)^1$	NN = 1.120; 1.163	−460.36701	−0.040; 0.125
linear Al·N_2·N_2;	AlN = 2.046; N...N = 3.441	9i(π); 13(σ)	−0.07; 3.04;
$^4\Sigma^-$ $(\sigma)^1(\pi)^2$	NN = 1.097; 1.132	−460.37692	−0.05; −0.71
linear N_2·Al·N_2[b];	AlN = 2.339	71(π_u); 79(σ_u)	0.13; 3.00;
$^4\Sigma_g^-$ $(\sigma_g)^1(\pi_u)^2$	NN = 1.107	−460.37996	−0.20; −0.31
C_{2v}, rectangular N_4, Al on top;	AlN = 4.054	15(a_1); 26(b_2)	−0.0186; 1.003
$^2B_1$ $(b_1)^1$	NN = 1.132; 3.555	−460.46995	0.004; 0.001
C_{2v}, T-shaped, NN·Al·(N_2);	AlN = 4.081; 3.468	26i(b_2); 4(b_1)	−0.04; 1.01
$^2B_2$ $(b_2)^1$	NN = 1.132; 1.29	−460.47026	−0.03; −0.04
linear N_2·Al·N_2; $^2\Pi_u$ $(\pi_u)^1$	AlN = 3.514	3, 14(π_u); 37(σ_g)	−0.06; 1.01;
	NN = 1.130	−460.47132	−0.03; −0.04
C_{2v} V-shaped; $^2B_1$ $(b_1)^1$	AlN = 3.421	24(a_1); 37(b_2)	−0.05; 1.01;
	NN = 1.130, 3.263	−460.47237	−0.03; −0.05

[a] The near-tetrahedral N_4 structure with Al at a vertex also converged to this structure (see text). [b] The $(a_1)^1(b_1)^1(a_1)^1$ $^4B_1$ state of near-V-shaped Al·(N_2)$_2$ was optimized also to this linear state.

TABLE 7: Optimized Geometrical Parameters (Å), Computed Harmonic Vibrational Frequencies (cm^{-1}), Total Electronic Energies (E_e in hartrees), Charge (q), and Spin (s) Densities of Various Electronic States of the Al·N_4 Ring Structure at the QCISD/aug-cc-pVDZ Level of Calculation

state	configuration/E_e(au)	optimized geometry (Å)	frequency (cm^{-1})	q_{Al}; s_{Al}/q_N; s_N
$^2A_1$	$(a_1)^1$ 25 points from MP2	Al = 4.721	not optimized (falling apart)	0.010; 1.008
		NN = 1.115; 5.239		0.08; −0.009
$^2B_2$	$(b_2)^1$[a]			
$^2B_1$	$(b_1)^1$ 25 points from MP2[b]	AlN = 3.596	not optimized	−0.037;1.010
		NN = 1.115; 4.266		−0.038; −0.018
$^4A_1$	$(a_2)^1(b_2)^1(b_1)^1$	AlN = 2.140	Qcisd excessive iterations	0.482; −0.154
	−460.21809	NN = 1.418; 1.259		−0.204; 1.626
$^4B_1$	$(a_2)^1(b_2)^1(a_1)^1$	AlN = 1.905	Qcisd excessive iterations	0.525; −0.023
	−460.20517	NN = 1.471; 1.237		−0.246; 1.611
$^4A_2$	$(b_2)^1(b_1)^1(a_1)^1$	AlN = 2.189	97.9(b_2); 165.0(b_1)	0.610; 0.151
	−460.29876	NN = 1.246; 1.361		−0.180; 1.548
$^4B_2$	$(a_2)^1(b_1)^1(a_1)^1$	AlN = 1.941	Qcisd excessive iterations	1.078; 0.905
	−460.22508	NN = 1.426; 1.292		−0.478; 1.048

[a] Very large spin contamination ($\langle S^2 \rangle = 1.95$). [b] Became a V-shaped structure; unoptimized after 25 points with AlN = 3.596 Å (see text).

consistent at all levels of calculation and hence should be reliable. In this connection, one of the most important conclusions from the present investigation is as follows. The stabilization of the LUMOs of bonding combinations of N_2 antibonding orbitals by orbital mixing with the appropriate Al valence p orbitals and the excitation schemes of promoting electrons from the HOMOs of antibonding combinations of N_2 bonding orbitals to the LUMOs, as proposed in ref 27, have been shown to be useful in obtaining desirable states/structures of AlN_4, which could be potential precursors of HEDM.

Other than ring structures, there are other structures that have well-bound quartet states. However, before they are discussed, the computed electronic energy changes, ΔE_e, for the decomposition reaction of an AlN_4 ring structure is considered first. The $^4A_2$ state, which is the lowest quartet state obtained and the only ring structure whose vibrational frequencies have been successfully calculated at the QCISD level (Table 7), was chosen in the following decomposition reaction. (The experimental r_e of 1.097685 Å was used in the calculation on N_2; see also later text for the possible reaction path on the energy hypersurfaces.)

$$AlN_4\ (^4A_2\ \text{5-membered ring}) \rightarrow Al\ (\tilde{X}^2P) + 2N_2\ (\tilde{X}^1\Sigma_g^+)$$

The results obtained at the RCCSD(T) level with different basis sets are shown in Table 9. First, from the computed ΔE_e values shown in Table 9, it can been seen that the contribution from triple excitations to the computed energy change for the decomposition reaction is significant. The computed ΔE_e values at the RCCSD(T) level with different basis sets are consistently 7.7 kcal/mol less negative than the RCCSD values. The consistency of the computed contributions from triples with different basis sets suggests that the contribution from triples obtained with a smaller basis set can be used as an approximation for the same contribution with a larger basis set, with little loss of accuracy. This approach was employed for larger clusters, where inclusion of triples in the CCSD calculations becomes

TABLE 8: Optimized Geometrical Parameters (Å), Computed Harmonic Vibrational Frequencies (cm^{-1}), Total Electronic Energies (E_e in hartrees), Charge (q), and Spin (s) Densities of Various Electronic States of Other AlN_4 Structures at the QCISD/aug-cc-pVDZ Level of Calculation

structure	state/configuration/E_e	optimized geometry (Å)	frequency (cm^{-1})	q_{Al}; s_{Al}/q_N; s_N
C_{2v} near-tetrahedral N_4;	$^4A_1$ $(b_2)^1(a_1)^1(b_2)^1$	AlN = 3.352	481i(b_1); 29(b_1)	−0.05; 1.01/−0.00;
Al at side	−460.12441	NN = 1.541, 1.443		−0.17, 0.03; 1.17
$N(N_3)$·Al C_{3v};	$^4A_1$ $(e)^2(a_2)^1$	AlN = 2.194	145(e); 324(a)	0.69;−0.07/−0.30;
Al at face	−460.18327	NN = 1.352; 2.277		1.29, 0.22; −0.80
C_{2v} near-tetrahedral N_4;	$^4A_2$ $(b_2)^1(b_1)^1(a_1)^1$	AlN = 2.226	162(b_2); 187(b_1)	0.60; 0.04/−0.16;
Al at side	−460.20821	NN = 1.909, 1.453		0.50, −0.14; 0.98
C_{2v} rectangular N_4;	$^4B_2$ $(b_2)^1(b_1)^1(b_1)^1$	AlN = 2.479	814i(b_1); 121i(b_1)	0.53; 0.25/−0.13;
Al on top	−460.24746	NN = 1.225; 2.008		0.69
C_{2v} T-shaped	$^4A_2$ $(a_1)^1(b_2)^1(b_1)^1$	AlN = 2.123; 3.179	10(b_2); 44(a_1)	0.54; 2.24/−0.32;
(N_2)·Al···NN	−460.37552	NN = 1.179; 1.115		0.42, 0.01;−0.06
linear N_2·Al·N_2	$^4\Sigma_g^-$ $(\sigma_g)^1(\pi_u)^2$	AlN = 2.181	174i(σ_u); 56(π_u)	0.27; 2.97/−0.29;
(see footnote)[a]	−460.39547	NN = 1.123		−0.56, 0.16; 0.59
linear N_2·Al··· N_2	$^4\Sigma^-$ $(\sigma)^1(\pi)^2$	AlN = 1.888; 3.333	24(π); 41(σ)	0.25; 2.82/−0.49;
	−460.40027	NN = 1.146; 1.115		−0.95, 0.20; 1.17
C_{2v} near-tetrahedral N_4;	$^2B_2$ $(b_2)^1$	AlN = 2.982	61i(b_2); 210(b_1)	0.55; 0.01/−0.08;
Al at side	−460.19961	NN = 1.996; 1.479		−0.13, −0.19; 0.63
C_{2v} rectangular N_4;	$^2B_1$ $(b_1)^1$	AlN = 4.332	SCF failure	−0.01; 1.00/0.00;
Al on top	−460.48765	NN = 1.115, 3.766		−0.00
linear N_2·Al·N_2	$^2\Pi_u$ $(\pi_u)^1$	AlN = 3.661	5, 14(π_u); 30(σ_g)	−0.05; 1.01
	−460.48883	NN = 1.115		

[a] The $^4B_1$ $(a_1)^1(b_1)^1(a_1)^1$ state of the C_{2v} V-shaped Al·$(N_2)_2$ structure was optimized also to this linear state/structure.

TABLE 9: Computed Electronic Energy Changes, ΔE_e, for the Reaction[a] AlN_4 $^4A_2$ five-membered ring → Al $\tilde{X}^2P$ + N_2 $\tilde{X}^1\Sigma_g^+$

ΔE_e(kcal/mol)	RCCSD	RCCSD(T)
aug-cc-pVTZ	−121.2	−113.5
aug-cc-pCVTZ[b]	−120.4	−112.8
aug-cc-pVQZ(no g)[c]	−122.7	−115.0

[a] The experimental r_e of 1.097685 Å was used in the calculation on N_2. [b] The aug-cc-pCVTZ basis set has the standard aug-cc-pVTZ basis set augmented with uncontracted s (exponents: 5.0, 1.923, 0.7396), p (5.0, 1.923), d (2.5), and f (2.0) functions for the Al $2s^22p^6$ core electrons. The RCCSD(T) calculations have only the 1s orbitals of Al and N frozen in the correlation treatment. The total number of basis functions for AlN_4 is 255. [c] The total number of basis functions for AlN_4 is 314.

too expensive (see later text). Second, core−core and core−valence correlation effects were considered by including the Al 2s2p core in the correlation treatment with an aug-cc-pCVTZ basis set designed in this work (see footnote a of Table 9). It can be seen that their contributions to ΔE_e are negligibly small (0.8 kcal/mol less negative). Therefore, core effects on computed ΔE_e values are ignored from here onward. Third, basis set effects on the computed ΔE_e values are shown to be reasonably small, with the aug-cc-pVTZ basis set giving a value of ΔE_e, which is 1.5 kcal/mol less negative than that obtained with the aug-cc-pVQZ(no g) basis set. Fourth, basis set superposition errors (BSSE) have been ignored in the evaluation of ΔE_e for decomposition reactions throughout the present study. This is because the decomposition products and the reactant have very different geometrical and electronic structures. It is felt that the commonly used counterpoise correction scheme[48] would be inappropriate.[49] At the same time, the effects of BSSE and larger basis size on the computed ΔE_e values are expected to be in opposite directions and hence would cancel each other at least to a certain extent. Finally, it is concluded that the computed values of ΔE_e shown in Table 9 suggest that the uncertainties associated with the value obtained at the highest level of calculation should be less than ±2 kcal/mol. In this connection, for the larger clusters considered in this work, it is anticipated that the computed exothermicities should be reliable to ca. ±2 kcal/mol if the ΔE_e values for the decomposition reactions are calculated at the RCCSD(T)/aug-cc-pVTZ level.

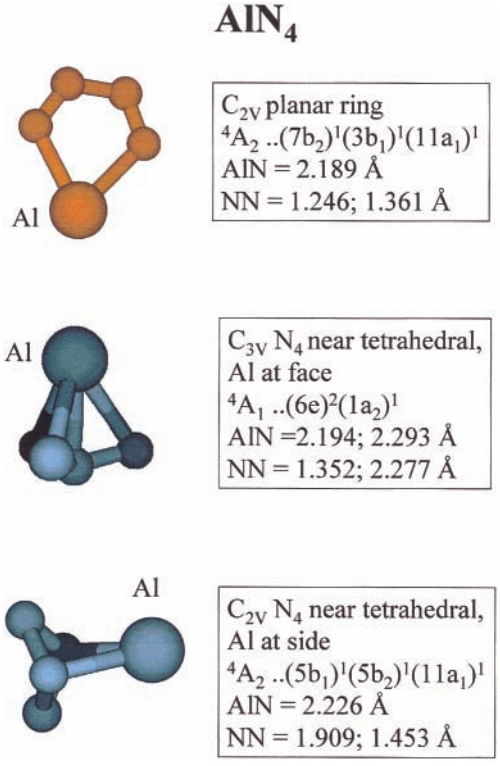

Figure 1. Some structures of AlN_4 studied in this work (see text).

Some computed thermodynamic constants for the decomposition of AlN_4 (the $^4A_2$ state of the ring structure) obtained at the RCCSD(T)/aug-cc-pVQZ(no g)//QCISD/aug-cc-pVDZ level, within the harmonic oscillator−rigid rotor approximation, are given below:

$$\Delta H(0\ \text{K}) = -116.6\ \text{kcal/mol}$$
$$\Delta H(298\ \text{K}) = -115.5\ \text{kcal/mol}$$
$$\Delta S = 55.1\ \text{cal/mol·K}$$
$$\Delta G(298\ \text{K}) = -131.9\ \text{kcal/mol}$$

Quartet states of linear, T-shaped, rectangular N_4 and near-tetrahedral N_4 structures of AlN_4 have also been studied (Tables

TABLE 10: Optimized Geometrical Parameters (Å), Computed Harmonic Vibrational Frequencies (cm^{-1}), Total Electronic Energies (E_e in hartrees), Charge (q), and Spin (s) Densities of Various Electronic States of Some Al_2N_4 Structures (see text) Obtained at the B3LYP and MP2 Levels of Calculation[a]

structure	state/configuration/E_e	optimized geometry (Å)	frequency (cm^{-1})	q_{Al}; s_{Al}/q_N; s_N
B3LYP/aug-cc-pVDZ				
D_{2h} planar; Al atoms	^1A_g	AlN = 2.171	48(b_{2u}); 65(b_{3u})	0.19/−0.10
at shorter NN sides	−703.85038	NN = 1.173; 2.671		
MP2/aug-cc-pVDZ				
D_{2h} planar; Al atoms	$^3B_{3u}$ $(b_{1u})^1(b_{2g})^1$	AlN = 2.168	170(b_{3u}); 246(a_u)	0.47; 0.34/
at longer N···N sides	−702.40824	NN = 1.193; 2.554		−0.23; 0.31
D_{2h} planar; Al atoms	$^3B_{1u}$ $(a_g)^1(b_{1u})^1$	AlN = 1.881	177(b_{3u}); 227(a_g)	0.89; 1.18/
at longer N···N sides	−702.40416	NN = 1.288; 2.884		−0.45; −0.09
D_{2h} planar; Al atoms	^1A_g	AlN = 2.150	62(b_{3u}); 83(b_2u)	0.48/−0.24
at shorter NN sides	−702.36551	NN = 1.215; 2.339		
D_{2h} planar; Al atoms	$^3B_{3u}$ $(b_{1u})^1(b_{2g})^1$	AlN = 2.478	61(b_{1u}); 154(b_{2g})	0.35; 0.39/
above and below	−702.36148	NN = 1.210; 2.710		−0.18; 0.31
D_{2h} planar; Al atoms	$^3B_{2u}$ $(b_{2u})^1(a_g)^1$	AlN = 1.918	95(a_g); 141(b_{3u})	0.65; 0.47/
at longer N···N sides	−702.28572	NN = 1.406; 2.814		−0.33; 0.27
MP2/6-311+G(3df)				
D_{2h} planar; Al atoms	$^3B_{1u}$ $(b_{1u})^1(a_g)^1$	AlN = 1.836	183(b_{3u}); 232(a_g)	0.71; 0.99/
at longer N···N sides	−702.59131	NN = 1.278; 2.813		−0.36; 0.00
D_{2h} planar; Al atoms	$^3B_{3u}$ $(b_{1u})^1(b_{2g})^1$	AlN = 2.112	256(b_{3g}); 265(a_g)	0.35; 0.27/
at longer N···N sides	−702.58086	NN = 1.177; 2.494		−0.18; 0.37
D_{2h} planar; Al atoms	^1A_g	AlN = 2.080	66(b_{3u}); 92(b_{2u})	0.38/−0.19
at shorter NN sides	−702.53822	NN = 1.201; 2.299		
D_{2h} planar; Al atoms	$^3B_{3u}$ $(b_{1u})^1(b_{2g})^1$	AlN = 2.442	65(b_{1u}); 135(b_{2g})	0.35; 0.36/
above and below	−702.52741	NN = 1.196; 2.646		−0.18; 0.32
D_{2h} planar; Al atoms	$^3B_{2u}$ $(b_{2u})^1(a_g)^1$	AlN = 1.867	89(a_g); 154(b_{3u})	0.42; 0.34/
at longer N···N sides	−702.46545	NN = 1.352; 2.419		−0.21; 0.33

[a] Stationary points, which are saddle points, have not been included in this table; see text.

4, 6, and 8). At the MP2 level, all the quartet states/structures considered are true minima, except two that are saddle points—the linear $Al{\cdot}N_2{\cdot}N_2$ $^4\Sigma^-$ state and the $^4A_2$ state of the structure with a near-tetrahedral N_4 group with Al at a face (Table 6). In addition, most of these quartet states are well bound, with short computed AlN bond lengths and reasonably large vibrational frequencies. However, at the QCISD level, only the $^4A_1$ and $^4A_2$ states of the near-tetrahedral N_4 structures with Al at a face and a side, respectively (Figure 1) have all real computed vibrational frequencies and hence are undoubtedly stable minima. Other quartet states, which are true minima at the MP2 level, have computed imaginary vibrational frequencies or face SCF convergence problems in the QCISD vibrational frequency calculations (Table 8). At this point, it may be appropriate to note that a computed imaginary vibrational frequency at a stationary point on the energy hypersurface is usually indicative of a saddle point. However, in numerical second derivative calculations at the QCISD level for an excited state, SCF calculations at a geometry displaced from the optimized geometry can land on the surface of a nearby state of the same symmetry in the lower-symmetry point group of the displaced geometry, with energy lower than that of the stationary point. This could lead to SCF convergence problems, QCISD iteration problems, imaginary or unphysical computed vibrational frequencies. Consequently, obtaining an imaginary frequency in a QCISD frequency calculation for an excited electronic state may or may not be indicative of a saddle point on the energy hypersurface. These kinds of problems/uncertainties in numerical second derivative calculations for excited states also occur in QCISD frequency calculations of larger clusters, as will be discussed later.

Laying aside states/structures with computed imaginary vibrational frequencies at the QCISD level, the results of the $^4A_1$ and $^4A_2$ states of the near-tetrahedral N_4 structures with Al at a face and a side, respectively, obtained at the B3LYP, MP2, and QCISD levels of calculation are reasonably consistent (Tables 4, 6, and 8). Hence, they are concluded to be reliable. It should be noted that the tetrahedral structure is the lowest-energy structure of singlet N_4 (see refs 1, 18, and 50 and reference therein). Here, the $^4A_1$ and $^4A_2$ states of the near-tetrahedral N_4 structures with Al at a face and a side, respectively, actually have their N_4 structures distorted significantly from a tetrahedral structure (Figure 1), suggesting strong interaction between Al and N_4. Nevertheless, the computed NN bond lengths in these two states/structures of AlN_4 are long (>1.34 Å; Tables 4, 6, and 8) and similar in magnitude to that of the singlet tetrahedral N_4 structure (1.478 Å) reported previously,[18] suggesting the presence of highly activated NN bonds. The computed charge and spin densities of these two states/structures show significant charge transfer from Al to N_4 and also delocalization of three unpaired electrons mainly on N_4. The molecular orbitals of these states/structures will be considered later.

Al_2N_4. The computed results are summarized in Tables 10 and 11. For the sake of simplicity, only states/structures that are true minima are included in Table 10. First, at the B3LYP level, all the triplet states/structures considered were either found to be saddle points or not optimized after a large number of searches (>50) in the geometry optimization calculation. However, with the MP2 and QCISD methods, four triplet states/structures were obtained (Tables 10 and 11). This shows the inadequacy of the density functional method for Al_2N_4.

Second, a singlet state/structure of Al_2N_4 has been obtained at all levels of calculations (Tables 10 and 11). This ^1A_g state has a short computed AlN bond length (<2.18 Å), and the computed charge densities show nontrivial charge transfer from Al to N_4. However, the computed intramolecular NN bond lengths are short, and the computed low vibrational frequencies are relatively small (ca. 60 cm^{-1}), suggesting small activation of the N_2 group and a relatively shallow minimum. The computed ΔE_e, $\Delta H^{0\ K}$, and $\Delta H^{298\ K}$ values at the RCCSD(T)/aug-cc-pVQZ(no g)//QCISD/aug-cc-pVDZ level for the decomposition reaction of Al_2N_4 (^1A_g) → 2Al + N_2 are −8.3, −10.5, and −8.9 kcal/mol, respectively. The energy release per N_2

TABLE 11: Optimized Geometrical Parameters (Å), Computed Harmonic Vibrational Frequencies (cm^{-1}), Total Electronic Energies (E_e in hartrees), Charge (q), and Spin (s) Densities of Various Electronic States of Some Al_2N_4 Structures[a] Obtained at the QCISD/aug-cc-pVDZ Level of Calculation

structure	state/configuration/E_e	optimized geometry (Å)	frequency (cm^{-1})	q_{Al}; s_{Al}/q_N; s_N
D_{2h} planar; Al atoms	$^3B_{3u}$ $(b_{1u})^1(b_{2g})^1$	AlN = 4.344	*b*	−0.01; 1.00/0.01
above and below	−702.41021	NN = 1.116; 3.733		−0.00
D_{2h} planar; Al atoms	$^3B_{3u}$ $(b_{1u})^1(b_{2g})^1$	AlN = 2.193	427i(b_{2u}); 99(b_{3u})	0.45; 0.35/−0.22;
at longer N···N sides	−702.40321	NN = 1.162; 2.547		0.33
D_{2h} planar; Al atoms	^1A_g	AlN = 2.141	55(b_{2u}); 63(b_{3u})	0.47/−0.23
at shorter NN sides	−702.36103	NN = 1.189; 2.324		
D_{2h} planar; Al atoms	$^3B_{1u}$ $(a_g)^1(b_{1u})^1$	AlN = 1.974	*c*	0.75; 0.85/−0.37;
at longer N···N sides	−702.32422	NN = 1.186; 2.523		0.07
D_{2h} planar; Al atoms	$^3B_{2u}$ $(b_{2u})^1(a_g)^1$	AlN = 1.892	*c*	0.78; 0.55/−0.39;
at longer N···N sides	−702.19210	NN = 1.281; 1.953		0.22

[a] See text. [b] The first displacement took more than 10 CPU day to finish; unable to complete frequency calculation. [c] Excessive QCISD iteration.

TABLE 12: Optimized Geometrical Parameters (Å), Computed Harmonic Vibrational Frequencies (cm^{-1}), Total Electronic Energies (E_e in hartrees), Charge (q), and Spin (s) Densities of Various Electronic States of AlN_5 Ring Structures[a] at the B3LYP/aug-cc-pVDZ Level of Calculation[b]

structure; states	geometry (Å)	frequency (cm^{-1}); E_{rel} (kcal/mol)	charge; spin
Al·N_2N_3;	AlN = 2.020	70b_2; 75b_1	Al(0.22; 2.02)
$^3B_1$, a_1b_1	NN = 1.333; 1.304; 1.346	69.8	N(−0.11; −0.06, 0.02; −0.01, −0.05; 0.11)
Al·NN_4;	AlN = 1.900	101b_2; 166b_1	Al(0.33; 2.03)
$^3B_1$, a_1b_1	NN = 1.338; 1.304; 1.344	67.9	N(0.98; −0.15, −0.53; 0.05, −0.12; 0.013)
AlN_5;	AlN = 1.934	143b_1; 268a_2	Al(0.63; 0.74)
$^3B_2$, a_1b_2	NN = 1.230; 1.350	54.8	N(−0.35; 0.35, 0.09; 0.23, −0.11; 0.09)
Al·N_2N_3;	AlN = 2.144	44b_2; 103b_1	Al(0.30)
$^1A_1$	NN = 1.325; 1.315; 1.337	1.1	N(−0.08, −0.05, −0.03)
AlN_5;	optimized to Al·N_2N_3		
$^1A_1$			
Al·NN_4;	AlN = 1.990	64b_2; 114b_1	Al(0.28)
$^1A_1$	NN = 1.337; 1.301; 1.351	0	N(0.99, −0.5, −0.13

[a] All have C_{2v} symmetry. [b] (Al·NN_4) and (Al·N_2N_3) are with an N_5 five-membered ring, and Al is at a vertex or a side; (AlN_5) is with a six-membered ring.

molecule from the decomposition reaction at 298 K is less than 5 kcal/mol. The low calculated exothermicity clearly shows that this state/structure is not a suitable candidate for HEDM.

Third, when the four triplet states/structures obtained are considered, two of them are lower in energy than the ^1A_g state at the MP2 and QCISD levels. However, at the MP2/aug-cc-pVDZ level, the lowest state/structure is the $^3B_{3u}$ state (the Al atoms are positioned at the longer N···N sides), with a $^3B_{1u}$ state only 2.6 kcal/mol higher in energy (Table 10). At the MP2/6-311+G(3df) level, the $^3B_{1u}$ state/structure becomes the lowest state, with the $^3B_{3u}$ state 6.6 kcal/mol higher. At the QCISD level, the $^3B_{3u}$ state (Al atoms above and below rectangular N_4) becomes the lowest state/structure, whereas the $^3B_{1u}$ state is now higher in energy than the ^1A_g state (Table 11). It should be noted that the $^3B_{3u}$ state (Al atoms above and below N_4) has a relatively long AlN bond length of >2.4 Å at the MP2 level, and at the QCISD level, the AlN distance increases to 4.3 Å and the $^3B_{3u}$ state becomes a very weakly bound state. Perhaps including triples in the QCISD calculation may stabilize this state. It should also be pointed out that the optimized geometrical parameters of the $^3B_{2u}$ state/structure (with the Al atoms positioned at the longer N···N sides) obtained using the aug-cc-pVDZ and 6-311+G(3df) basis sets at the MP2 level differ significantly, suggesting a relatively large basis set effect on geometry for this state/structure. In addition, the QCISD geometrical parameters of this state/structure also differ significantly from the MP2 parameters. In summary, it seems clear that for Al_2N_4 the demand on both the basis set and theoretical method employed in the calculation is higher than for AlN_4.

Fourth, from the present investigation, the lowest state/structure of Al_2N_4 is probably a triplet state rather than a singlet state, though higher-level calculations would be required to identify its structure. This leads to one major difference between Al_2N_4 and AlN_n systems. AlN_n clusters have their low-spin states significantly lower in energy than their high-spin states, and the ground state is almost certainly a low-spin state (see also later text). However, Al_2N_4 has its singlet and triplet states at comparable energies, and probably its ground state is a triplet state.

Finally, the highest-energy $^3B_{2u}$ state/structure obtained in this study is most relevant to the present investigation. The computed AlN and NN bond lengths are short and long, respectively, suggesting strong interaction between Al and N_2 and strong activation of NN bonds. The trends in the computed geometrical parameters and charge densities obtained at different levels of calculations suggest that electron correlation enhances metal−polynitrogen interaction and stabilizes the rectangular N_4 structure. The computed ΔE_e, $\Delta H^{0\ K}$, and ΔH^{298K} values at the RCCSD(T)/aug-cc-pVQZ(no g) level (with the QCISD/aug-cc-pVDZ geometry and MP2/6-311+G(3df) vibrational frequencies) for the decomposition reaction of Al_2N_4 ($^3B_{2u}$) → 2Al + N_2 are −92.4, −98.4, and −95.4 kcal/mol, respectively. The energy release per N_2 of 48 kcal/mol at 298 K is quite large.

AlN_5. The computed results are summarized in Tables 12 to 14, and the different types of structures considered are shown in Figure 2. First, it should be mentioned that the singlet state of AlN_5 with Al on top of an N_5 five-membered ring was found to be a second-order saddle point on the B3LYP/aug-cc-pVDZ energy hypersurface. The geometry optimization was run as a $^1A'$ state in C_s symmetry with an initial geometry of a near-C_{5v} structure and the optimization converged to a C_{5v} structure. In addition, the $^3A'...(a')^1(a')^1$ state of the same initial structure

TABLE 13: Optimized Geometrical Parameters (Å), Computed Harmonic Vibrational Frequencies (cm^{-1}), Total Electronic Energies (E_e in hartrees), Charge (q), and Spin (s) Densities of Various Electronic States of AlN_5 Ring Structures[a] at the MP2/aug-cc-pVDZ Level of Calculation

structure; states	geometry (Å)	frequency (cm^{-1}); E_{rel} (kcal/mol)	charge; spin
$Al{\cdot}N_2N_3$;	AlN = 2.077	$103b_1$; $136b_2$	Al(0.49; 2.15)
$^3B_1$, a_1b_1	NN = 1.345; 1.279; 1.306	69.6	N(−0.39;0.04, 0.15;−0.26, −0.02; 0.29)
$Al{\cdot}NN_4$;	AlN = 1.929	$102b_2$; $136b_1$	Al(0.46; 2.21)
$^3B_1$, a_1b_1	NN = 1.343; 1.336; 1.346	62.5	N(0.71; −0.31, −0.48; 0.06, −0.11; 0.012)
AlN_5;	AlN = 1.848	$166b_1$; $350a_1$	Al(1.11;0.82)
$^3B_2$, b_2 a_1	NN = 1.232; 1.375	65.7	N(−0.32; 0.55, −0.91;−0.03, −0.28; 0.14)
$Al{\cdot}N_2N_3$;	AlN = 2.152	$86b_2$; $96b_1$	Al(0.54)
$^1A_1$	NN = 1.354; 1.337; 1.343	0.0	N(−0.31, 0.03, 0.01)
AlN_5;	AlN = 2.122	$359ib_2$; $140b_1$	Al(0.56)
$^1A_1$	NN = 1.211; 1.369	1.1	N(−0.19, 0.04, −0.27)
$Al{\cdot}NN_4$;	AlN = 2.008	$31b_2$; $97b_1$	Al(0.46)
$^1A_1$	NN = 1.346; 1.335; 1.349	0.7	N(0.66, −0.46, −0.10)

[a] All have C_{2v} symmetry. [b] ($Al{\cdot}NN_4$) and ($Al{\cdot}N_2N_3$) are with an N_5 five-membered ring, and Al is at a vertex or a side; (AlN_5) is with a six-membered ring.

TABLE 14: Optimized Geometrical Parameters (Å), Computed Harmonic Vibrational Frequencies (cm^{-1}), Total Electronic Energies (E_e in hartrees), Charge (q), and Spin (s) Densities of Some Selected States/Structures of AlN_5 at the QCISD/aug-cc-pVDZ Level of Calculation

structure; states	geometry (Å)	frequency (cm^{-1}); E_{rel} (kcal/mol)	charge; spin
$Al{\cdot}NN_4$;	AlN = 1.921	[a]65.0	Al(0.46; 2.22)
$^3B_1$, a_1b_1	NN = 1.338; 1.307; 1.353		N(0.71; −0.30, −0.46; 0.05, −0.12; 0.007)
AlN_5;	AlN = 1.947	[b]66.0	Al(0.94; 0.20)
$^3B_2$, a_1b_2	NN = 1.236; 1.361		N(−0.22; 0.16, −0.13; 0.06, −0.25; 0.05)
$Al{\cdot}NN_4$;	AlN = 1.990	$73b_2$; $104b_1$	Al(0.46)
$^1A_1$	NN = 1.341; 1.302; 1.362	−2.1	N(0.65, −0.43, −0.12)
$Al{\cdot}N_2N_3$;	AlN = 2.149	$51ib_2$; $88b_1$	Al(0.54)
$^1A_1$	NN = 1.339; 1.319; 1.331	0.0	N(−0.31, 0.04, 0.00)

[a] Numerical second derivative calculations failed. [b] Unable to finish numerical second derivative calculations because of time constraints.

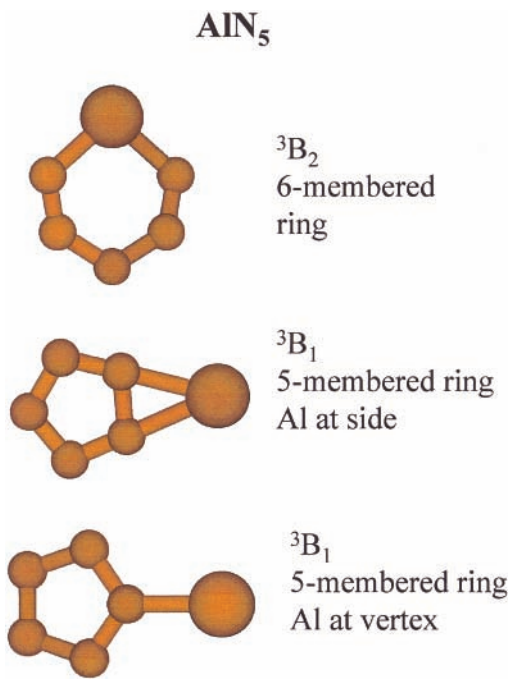

Figure 2. Some structures of AlN_5 studied in this work (see text).

optimized at the B3LYP/aug-cc-pVDZ level to a planar C_{2v} structure, with the Al atom moved from the top of the N_5 five-membered ring to a side (Figure 2). It appears that with Al, the η^5-N_5-type structure is not favored, at least at the B3LYP level. This is the case also for larger AlN_n clusters, which will be discussed later. Nevertheless, planar AlN_5 structures seem to be very stable, as can be seen from Tables 12 to 14. One main difference between AlN_4 and AlN_5 is that the former has mainly strongly bound quartet states (high-spin states) but the latter has as many strongly bound singlet states as triplet states (high- and low-spin states). Nevertheless, the singlet states/structures are consistently lower in energy than the triplet states for both AlN_4 and AlN_5, as mentioned above. Although the calculated relative energy order of the different AlN_5 states/structures, obtained at different levels of calculation, differ slightly, their optimized geometrical parameters, computed harmonic vibrational frequencies, and charge/spin densities are very consistent. All these results suggest that most of the low-lying singlet and triplet states of AlN_5 are reasonably well bound and have activated NN bonds. These states/structures could be potential candidates for precursors of HEDM. The calculated exothermicities of decomposition of some selected state/structures will be discussed later. At this point, it is concluded that Al appears to be a very suitable metal to be employed to stabilize polynitrogen species, particularly N_5 ring structures. The ability of this p-block metal to introduce both covalent and ionic interactions to a polynitrogen species has led to a large number of AlN_5-stabilized states/structures.

AlN_6 and AlN_7. For AlN_6 at the B3LYP/aug-cc-pVDZ level of calculation, there are two $^2A'$ states/structures—one with Al at a vertex (forming an AlN bond; boat-shaped $Al{\cdot}NN_5$) and one with Al at a side (boat-shaped $Al{\cdot}N_2N_4$)—that are true minima. In addition, the $^4B_2$ state (planar AlN_6, with a N_6 ring and Al bonded to NN) and two $^4A''$ states (N_6 ring of a boat shape, with Al bonded to a vertex and a side; see Figure 3) were also found to be true minima. However, at the MP2/aug-cc-pVDZ level of calculation, there is only one true minimum, which is a $^4A''$ state, with Al at a vertex, and the computed results are given in Figure 3. Other states/structures, which are

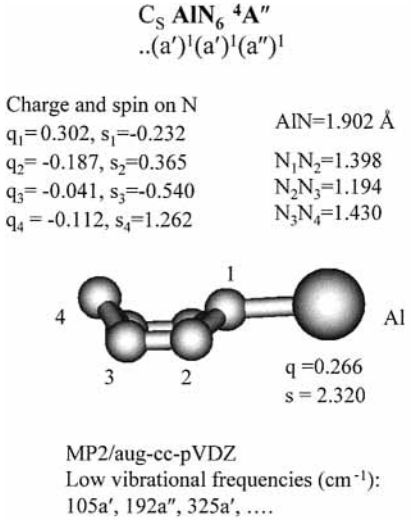

Figure 3. AlN_6 structure obtained in this work with a summary of the computed quantities at the MP2/aug-cc-pVDZ level of calculation (see text).

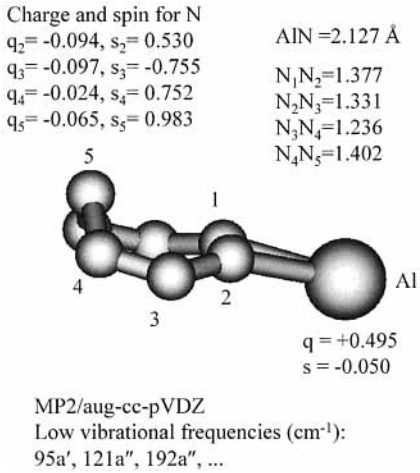

Figure 4. AlN_7 structure obtained in this work with a summary of the computed quantities at the MP2/aug-cc-pVDZ level of calculation (see text).

minima at the B3LYP level, become saddle points at the MP2 level. Perhaps the following results of planar η^6-N_6-type structures, with Al on top of a planar N_6 ring, obtained at the B3LYP/aug-cc-pVDZ level of calculation should be noted. Geometry optimization of the quartet state with a C_{6v} structure faced persistent SCF convergence failures. The corresponding doublet state was not converged after 100 points of searches in the geometry optimization. The last geometry reached the displacement threshold, but the gradients were very large.

For AlN_7 at the B3LYP/aug-cc-pVDZ level of calculation, the following true minima were found: an $^1A'$state (a near-planar N_7 ring with Al bonded to a side, slightly above the N_7 ring), a $^3B_1$ state (AlN_7 planar eight-membered ring), and an $^3A''$ state (an N_7 boat-shaped ring with Al bonded to a side; see Figure 4). However, at the MP2 level of calculation, only the $^3A''$ state/structure is a true minimum, and the computed results are given in Figure 4. Other minima obtained at the B3LYP level have either became saddle points or faced geometry optimization problems (unoptimized after a very large number of searches) at the MP2 level of calculation. A large number of other singlet and triplet states/structures of AlN_7, including planar η^7-N_7-type structures, were studied at the B3LYP/aug-cc-pVDZ level of calculation. Although some of them were found to be saddle points of various orders, the rest either fell apart or were not optimized after a large number of searches in the geometry optimization.

In summary, for AlN_6 and AlN_7, at least one stable high-spin state/structure was obtained for each cluster at both the B3LYP and MP2 levels of calculation. The details of the computed results for these states/structures at the MP2 level are given in Figures 3 and 4, respectively. The computed geometrical parameters and vibrational frequencies at the B3LYP level are very similar to those obtained at the MP2 level, suggesting that these results are reasonably reliable. We note that the computed $\langle S^2 \rangle$ values for the AlN_7 $^3A''$ state at the MP2 (B3LYP) levels are 2.53 (2.03), suggesting considerable spin contamination in the UHF wave function at the MP2 level but negligible spin contamination at the B3LYP level. However, the consistency between the B3LYP and MP2 results suggests that the effects of spin contamination on these results are probably insignificant. From the computed $\langle S^2 \rangle$ values, spin contamination is not serious for most of the open-shell states reported in this work. From the present investigation, it is concluded that a boat-shaped N_n structure is preferred over a planar structure for an AlN_n system when n is larger than 5. The molecular orbitals of these systems will be examined in the following section to understand the stability of these structures.

Molecular Orbitals. The highest occupied molecular orbitals (HOMOs) of the Al_2N_4 and AlN_n (n = 4 to 7) clusters have been inspected. Although all the geometry optimization calculations of open-shell species carried out in this work employed unrestricted-spin (UHF) wave functions, for the sake of simplicity, the molecular orbitals of restricted-spin wave functions (i.e., ROHF wave functions for open-shell species) are considered in the following discussion. The HOMOs of the ring structures of different quartet states of AlN_4 will not be discussed further because they follow exactly what was postulated in ref 27 and have been discussed above.

The HOMOs for the two near-tetrahedral N_4 structures with Al at a face and a side are shown in Figures 5 and 6, respectively. It should be noted that the near-tetrahedral N_4 structure with Al at a vertex is not stable. Geometry optimization on the C_{3v} structure with Al at a vertex ended with the structure of Al at a face. The N atom on the C_3 axis moved away from Al and went through the N_3 plane, ending with the N_3 plane nearer to Al than the N atom on the C_3 axis (i.e., inversion of the Al·NN_3 structure to Al·N_3N). From Figures 5 and 6, it can be seen that, for both structures with Al at a face and a side, respectively, HOMO 19 is essentially Al 3s. Al 3p involvement in the HOMOs shown is small, leading to the computed charge densities of ca. 0.6 on Al (Tables 6 and 8). At the same time, the three singly occupied molecular orbitals (SOMOs; HOMOs 20, 21, and 22) for the two structures are localized mainly on N_4 in accordance with the very small computed spin densities on Al. In this connection, these two structures may be considered as $Al^+N_4^-$, with N_4^- in an excited quartet state.

For the structure with Al at a face (Figure 5), HOMO 22 is almost completely antibonding, and the two degenerate pairs of HOMOs 17, 18 $(5e)^4$ and 20, 21 $(6e)^2$ are mixtures of bonding and antibonding combinations. Whereas the strongest bonding interaction between Al and N appears in HOMO 19, a slight bonding interaction between Al and N_4 can be found in HOMO 13. For the structure with Al at a side (Figure 6), whereas HOMOs 20 and 21 are nonbonding, HOMO 22 is essentially antibonding. The involvement of Al 3p in all the HOMOs shown in Figure 6 appears to be even smaller than that in Figure 5 of the structure with Al at a face. The only HOMO with the

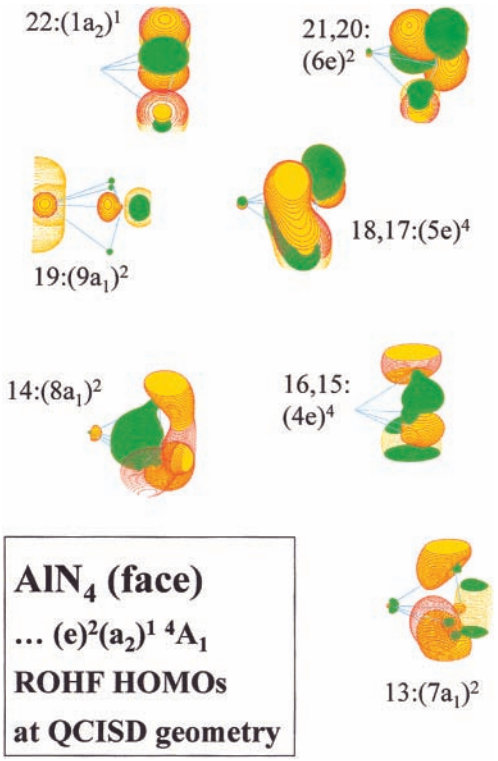

Figure 5. Some HOMOs of the $^4A_1$ state of AlN_4, a near-tetrahedral N_4 with Al at a face structure (see text).

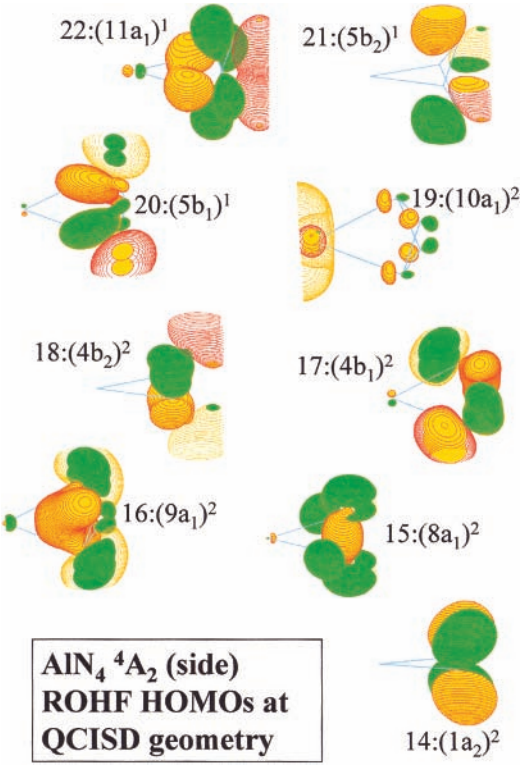

Figure 6. Some HOMOs of the $^4A_2$ state of AlN_4, a near-tetrahedral N_4 with Al at a side structure (see text).

structure of Al at a side, which shows possible bonding interaction between Al and N_4, is HOMO 16. In summary, from the HOMOs of both structures shown in Figures 5 and 6, whereas the destabilizing orbitals with strong antibonding character are SOMOs, most of the doubly occupied HOMOs possess bonding character in the N_4 molecular fragment. These

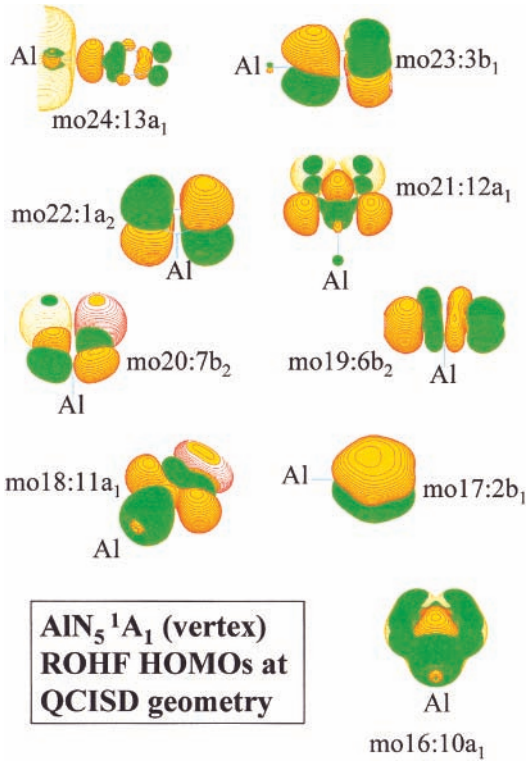

Figure 7. Some HOMOs of the $^1A_1$ state of AlN_5, an N_5 ring with Al at a vertex structure (see text).

electronic configurations are generally in accordance with the molecular orbital schemes proposed in ref 27 for some quartet states of MN_4 ring structures, although the HOMOs of the near-tetrahedral N_4 structures are very different from those of the ring structures.

The HOMOs of the $^1A_1$ state of the AlN_5 ring structure (Figure 7) can be compared with the published HOMOs of N_5^- and NaN_5 in Figure 1 of ref 32. In the case of N_5^- and NaN_5, their eight highest HOMOs are almost identical, with negligible differences between those of N_5^- and NaN_5, because there is no involvement of Na 3s in any of these HOMOs of NaN_5, giving a purely ionic picture of $Na^+N_5^-$. These eight HOMOs in N_5^- correspond to HOMOs 16 to 23 of AlN_5 in Figure 7, though the orders of these orbitals in N_5^- and AlN_5 are different, as will be discussed. For AlN_5, the highest HOMO 24 ($13a_1$), which is essentially Al 3s, has significant Al $3p_z$ mixing and also N_5 contributions. The presence of this HOMO has affected the orbital order of the HOMOs localized on N_5 in AlN_5, as compared with that in NaN_5. The highest HOMO in NaN_5 is now HOMO 18 ($11a_1$) in AlN_5. The lowering of the relative position of this HOMO in AlN_5 as compared to that in NaN_5 is clearly due to covalent interaction between Al and N_5. Specifically, the interaction among the HOMOs of a_1 symmetry results in such an orbital order because of the presence of the extra HOMO 24 ($13a_1$) in AlN_5. Other than HOMO 24, HOMOs 16, 18, 21, and 23 also have small Al 3s and $3p_x$ contributions, though they are mostly antibonding in nature. The remaining HOMOs 17, 19, 20, and 22 have negligible contributions from Al and are almost identical to the corresponding orbitals in NaN_5.

The HOMOs of the $^3B_1$ state of Al·NN_4 (Al at a vertex of the N_5 ring) are very similar to those of the $^1A_1$ state of a similar structure (just discussed; Figure 7), except that there is an extra HOMO, the highest singly occupied molecular orbital (SOMO) 25, in the triplet state. The $^3B_1$ state has an electron excited

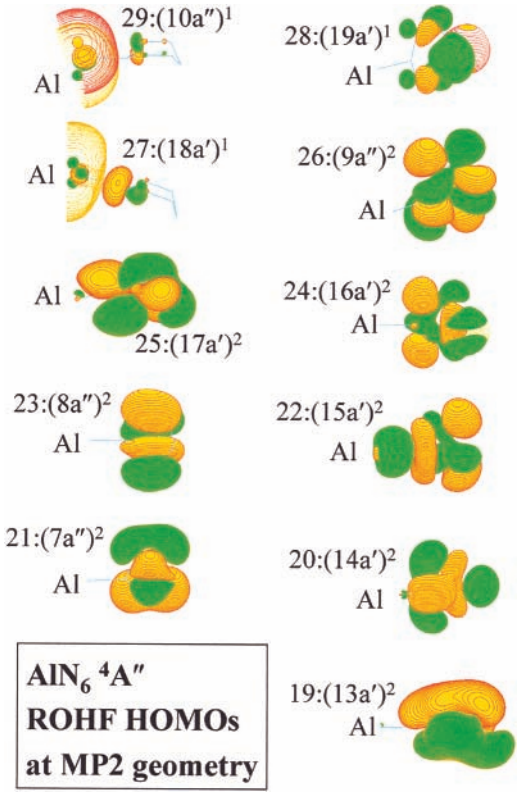

Figure 8. Some HOMOs of the $^4A''$ state of AlN_6, a boat-shaped N_6 with Al at a vertex structure (see text).

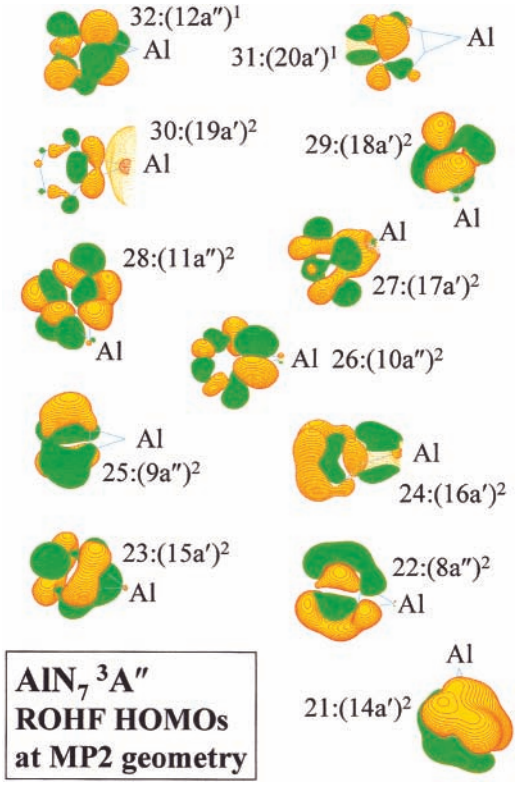

Figure 9. Some HOMOs of the $^3A''$ state of AlN_7, a boat-shaped N_7 with Al at a side structure (see text).

from the $13a_1$ orbital of the $^1A_1$ state to an unoccupied $4b_1$ orbital. The latter is essentially Al $3p_x$ but has significant contributions from a mixture of bonding and antibonding combinations of orbitals localized on N_5. The $^3B_1$ state with Al at a side of the N_5 ring has its HOMOs essentially similar to those of the $^3B_1$ state with Al at a vertex. As a result, the computed charge and spin densities of these two triplet states are also very similar. However, the HOMOs of the $^3B_2$ state with Al as part of the six-membered ring show significantly stronger mixing between Al and N_5 orbitals than do those in the two triplet states of the N_5 five-membered ring structures just considered. As a result, the computed charge and spin densities of the $^3B_2$ state of AlN_5 are considerably larger and smaller, respectively, than those of the two $^3B_1$ states of Al·NN_4 and Al·N_2N_3 (Tables 12, 13, and 14). All these observations show the ability of Al to introduce various degrees of covalency and/or ionicity in different states/structures of AlN_n, which stabilize a large number of them.

The HOMOs of AlN_6 and AlN_7 are shown in Figures 8 and 9. First, although both of these structures are nonplanar, with boat-shaped N_n structures, it is of interest to note that HOMO 19 of AlN_6 and HOMO 21 of AlN_7 are essentially π-type orbitals, similar to HOMO 17 in Figure 7 of planar AlN_5. It seems that although the N_n rings are nonplanar, some sort of π-electron system remains. Second, most of the doubly occupied HOMOs of AlN_6 and AlN_7 are quite similar and are mixtures of bonding and antibonding combinations. It appears that the boat-shaped structures have enabled a bonding interaction to occur in these HOMOs, which would be antibonding if the N_n rings are planar. This is most likely the reason for the stability of N_n boat-shaped structures for AlN_6 and AlN_7. Third, the major differences between AlN_6 and AlN_7 are their SOMOs, resulting in very different computed charge and spin densities on Al (Figures 3 and 4). Once again, this demonstrates the ability of Al to introduce different degrees of covalency and/or ionicity in AlN_n species.

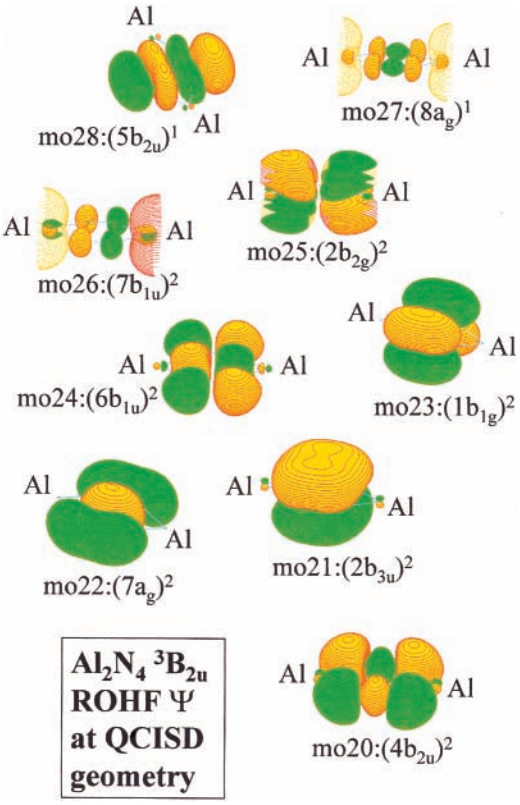

Figure 10. Some HOMOs of the $^3B_{2u}$ state of Al_2N_4, a rectangular N_4 with the Al atoms positioned at the long N···N sides structure (see text).

The HOMOs of the $^3B_{2u}$ state of Al_2N_4 are shown in Figure 10. In general, the electronic configuration of this state follows

TABLE 15: Summary of the Computed Exothermicities (ΔH^{298K} in kcal/mol) of the Decomposition of Some Aluminum Polynitrogen Compounds Obtained in This Work

method[a]	reactant, structure, state, electronic configuration	products[b]	$\Delta H^{298\ K}$
RCCSD(T)/AVQZ(no g)	AlN_4, C_{2v} ring, $^4A_2$, $(b_2)^1(b_1)^1(a_1)^1$	$Al + 2N_2$	−115.5
RCCSD(T)/AVQZ(no g)	AlN_4, C_{3v} Al·N_3N, $^4A_1$, $(e)^2(a_2)^1$	$Al + 2N_2$	−190.8
RCCSD(T)/AVQZ(no g)	Al_2N_4, C_{2h} AlN_2·N_2Al, ^1A_g	$2Al + 2N_2$	−8.9
RCCSD(T)/AVQZ(no g)	Al_2N_4, C_{2h} AlN_2·N_2Al, $^3B_{2u}$	$2Al + 2N_2$	−95.4
RCCSD(T)/AVQZ(no g)	AlN_5, C_{2v} Al·N_2N_3 (N_5 ring), $^1A_1$	$Al + {}^5/_2N_2$	−58.6
	as above	$AlN + 2N_2$	−4.2
RCCSD(T)/AVQZ(no g)	AlN_5, C_{2v} Al·N_2N_3 (N_5 ring), $^3B_1$, $(a_1)^1(b_1)^1$	$Al + {}^5/_2N_2$	−128.1
	as above	$AlN + 2N_2$	−75.5
RCCSD(T)/AVTZ[c]	AlN_6, C_s Al·NN_2N_2N (N_6 ring), $^4A''$ $(a')^1(a')^1(a'')^1$	$Al + 3N_2$	−226.0
RCCSD(T)/AVTZ[c]	AlN_7, C_s Al·$N_2N_2N_2N$ (N_7 ring), $^3A''$, $(a')^1(a'')^1$	$Al + {}^7/_2N_2$	−216.4
	as above	$AlN + 3N_2$	−162.3

[a] For AlN_4 and Al_2N_4, the QCISD/aug-cc-pVDZ geometries were employed in the RCCSD(T) single-point energy calculations. For larger species, the MP2/aug-cc-pVDZ geometries were used. AVQZ and AVTZ refer to the standard aug-cc-pVQZ and aug-cc-pVTZ basis sets, respectively. [b] The products considered are in their electronic ground states—Al ($\tilde{X}^2P$) and N_2 ($\tilde{X}^1\Sigma_g^+$)—except for AlN ($\tilde{A}^3\Sigma^-$), which was computed to be 0.06 kcal/mol above its ground state, AlN ($\tilde{X}^3\Pi$), at the RCCSD(T)/WMR level.[42] [c] The RCCSD(T)/AVTZ value was estimated from the RCCSD/AVTZ value (with the full aug-cc-pVTZ basis set, but without triples) and the contribution of the triples obtained from the RCCSD(T)/AVTZ(no f) calculations. The RCCSD(T) calculation with the full AVTZ basis set is beyond the computing capacity available to us (see text).

the molecular orbital schemes given in ref 27. Specifically, the singly occupied HOMO 28 is mainly an antibonding combination of N_2 bonding orbitals, whereas the doubly occupied HOMOs 24 and 25 are mainly bonding combinations of N_2 antibonding orbitals. In addition, HOMOs 26 and 27, which are mainly Al 3s and 3p, have bonding contributions from N_2-localized orbitals. All these doubly occupied HOMOs stabilize the rectangular N_4 structure.

Exothermicities of the Decomposition Reaction of AlN_n Systems. The calculated exothermicities of the decomposition reactions of various Al_2N_4 and AlN_n systems are summarized in Table 15, and they were evaluated assuming that the dissociation products are in their ground electronic states (for AlN, see footnote b of Table 15). First, for AlN_n systems, where n is an even number, it is expected that high-spin quartet states are metastable because low-lying doublet states are in general lower in energy than the quartet states and almost certainly the ground state is a weakly bound doublet state. This is the case, at least for AlN_4, though for AlN_n, where n is an even number larger than 4, low-lying doublet hypersurfaces may be repulsive because for AlN_6, no minimum of a doublet state/structure was found with certainty (see above). In this connection, the dissociation process from an AlN_n quartet state to the ground state of the dissociation products would very likely proceed via spin−orbit interaction at a suitable crossing between the quartet and doublet hypersurfaces. Because low-lying, weakly bound doublet states have long computed AlN bond lengths, whereas strongly bound quartet states have short computed AlN bond lengths, it would be reasonable to expect that such a crossing between the quartet and doublet surfaces would exist at an intermediate AlN bond length. Of course, further investigation is required to locate the exact position of such a crossing. Nevertheless, it is expected that once the dissociation reaction has gone over the barrier of such a crossing and landed on the weakly bound or even repulsive doublet surfaces of AlN_n, the decomposition to the dissociation products of $Al + ({}^n/_2)N_2$ would proceed either via a low barrier or spontaneously, respectively.

For AlN_n systems with an odd n, low-lying triplet states are in general also higher in energy than low-lying singlet states. However, at least for AlN_5, there are well-bound singlet states/structures with activated NN intermolecular bonds (significantly longer computed NN bond lengths than in N_2), which may be suitable candidates for precursors of HEDM. Nevertheless, whether for singlet or triplet states/structures, the dissociation pathways of AlN_n systems to N_2 molecules, where n is an odd number, are not immediately obvious. Considering simply the exothermicity of the overall dissociation to N_2 molecules, two decomposition reactions of AlN_n, with an odd n, have been considered (see Table 15):

$$AlN_7 \rightarrow AlN + 3N_2$$

and

$$AlN_7 \rightarrow Al + 3.5N_2$$

This follows what Gagliardi and Pyykko[30] did for the decomposition of ScN_7 ($ScN_7 \rightarrow ScN + 3N_2$ and $ScN_7 \rightarrow Sc + 3.5N_2$).

For Al_2N_4, the ground state is very likely a triplet state, and the singlet state obtained is now metastable. However, the decomposition of this singlet state to N_2 molecules is only slightly exothermic, as mentioned above. Nevertheless, the $^3B_{2u}$ state of Al_2N_4 may be a suitable candidate as a precursor of HEDM on the grounds of its large computed exothermicity discussed above. The short computed AlN bond lengths of this state (Tables 10 and 11) suggest that its decomposition pathway is likely via a crossing with a weakly bound triplet surface that has its minimum lower in energy and at a longer AlN bond length than does the $^3B_{2u}$ state.

For AlN_6 and AlN_7, RCCSD(T) calculations with the aug-cc-pVTZ basis set were found to be beyond the computing capacity available to us (the calculation of the triples required more than 2 GB of memory). The aug-cc-pVTZ(no f) basis set was used to estimate the contributions from triples (as mentioned above; see footnote c of Table 15). From Table 15, if the decomposition reaction of AlN_n, where n is an odd number, to $AlN + (n-1)/2N_2$ is ignored for the sake of simplicity, the exothermicities of all the reactions shown are larger than 100 kcal/mol for all the high-spin states of AlN_n listed. For AlN_5, the exothermicity of the decomposition from the $^1A_1$ state considered is 58.9 kcal/mol, which is not insignificant. To compare the exothermicities of all the species given in Table 15 on a common footing, the computed energy releases per N_2 molecule at 298 K are given Table 16. These values are in general significantly higher than those calculated for ScN_7 (the largest energy release per N_2 given in ref 30 for ScN_7 is 36 kcal/mol), suggesting that AlN_n systems are more favorable potential candidates as precursors of HEDM than ScN_7.

TABLE 16: Energy Release Per N_2 Unit at 298 K for the Decomposition Reaction $AlN_n \rightarrow Al + (^n/_2)N_2$

with even n	$\Delta H^{298\ K}$
Al_2N_4 D_{2h}, $^3B_{2u}$	−47.8
AlN_4 C_{2v} ring $^4A_2$	−57.8
AlN_4 C_{3v} near-tetrahedral N_4, Al at face, $^4A_1$	−95.8
AlN_6 C_s N_6-ring $^4A''$	−75.3
with odd n	**$\Delta H^{298\ K}$**
AlN_5 C_{2v} N_5-ring $1A_1$	−23.4
AlN_5 C_{2v} N_5-ring $3B_1$	−51.2
AlN_7 C_s N_7-ring $^3A'$	−86.6

Concluding Remarks

Low-lying high- and low-spin states of Al_2N_4 and AlN_n, for $n = 4$ to 7, have been studied by density functional and ab initio methods. The main purpose of these calculations is to search for states/structures that may be suitable candidates for precursors of HEDM. In the search for these states/structures of Al_2N_4 and AlN_n with $n = 4$ and 5, particularly those with planar ring structures, simple molecular orbital schemes have been followed on the basis of the consideration of bonding and antibonding combinations of N_2-localized π^* and π orbitals, respectively, as proposed previously.[27] It was found that these molecular orbital schemes worked reasonably well, and well-bound charge transfer states/structures with activated NN bonds were obtained following these schemes. For AlN_6 and AlN_7, such states/structures have also been obtained, and they were found to have N_n boat-shaped structures. Analysis of their HOMOs suggests that the N_n boat-shaped structures obtained have facilitated bonding interaction, particularly in N_n localized HOMOs, which would be antibonding if the N_n ring were planar. It appears that for AlN_n with n larger than 5, a boat-shaped structure is preferred to a planar structure.

Considering metal−polynitrogen interaction, the HOMOs and the computed spin and charge densities of the well-bound NN-activated states/structures of Al_2N_4 and AlN_n obtained in this study demonstrate clearly the ability of Al to introduce various degrees of covalency and/or ionicity into these clusters, which stabilize the polynitrogen system. In this connection, it should be mentioned that geometry optimization calculations were also carried out on N_n molecules at the B3LYP and MP2 levels with the aug-cc-pVDZ basis set, where $n = 5$, 6, and 7. The initial geometries of these optimization calculations were chosen from those of N_n units in well-bound states/structures obtained for AlN_n. All these optimizations ended as saddle points, with the N_n system falling apart or unoptimized after a large number of searches. It is clear that without Al, the N_n systems in AlN_n are unstable.

Following the success of the present study in obtaining states/structures of Al_2N_4 and AlN_n clusters, which may be suitable candidates for precursors of HEDM, further investigations are underway. They include studying other states/structures, particularly the larger clusters such as AlN_6 and AlN_7, which have not been considered in the present study, AlN_n, where n is larger than 7, and Al_nN_m systems, where n is larger than 2 and/or m is larger than 4. In addition, further investigations on the energy hypersurfaces of the Al_2N_4 and AlN_n complexes already investigated will be required in order to locate the energy barrier of the decomposition reactions discussed. Finally, the large computed energy releases per N_2 molecule of the AlN_n species obtained in the present study from decomposition reactions (to Al and N_2) by high-level ab initio calculations suggest strongly that they are potential precursors of high energy density materials.

Acknowledgment. Financial support from DERA (MOD, Fort Halstead, U.K.) and computational resources from EPSRC via the U.K. Computational Chemistry Facility are gratefully acknowledged.

References and Notes

(1) Bartlett, R. J. *Chem. Ind. (London)* **2000**, 140.
(2) Ha, T.-K.; Suleimenov, D.; Nguyen, M. T. *Chem. Phys. Lett.* **1999**, *315*, 327.
(3) Christe, K. O.; Wilson, W. W.; Sheehy, J. A.; Boatz, J. A. *Angew. Chem., Int. Ed.* **1999**, *38*, 2004.
(4) Chung, G.; Schmidt, M. W.; Gordon, M. S. *J. Phys. Chem. A* **2000**, *104*, 5647.
(5) Zheng, J. P.; Waluk, J.; Spanget-Larsen, J.; Blake, D. M.; Radziszewski, J. G. *Chem. Phys. Lett.* **2000**, *328*, 227.
(6) Manaa, M. R. *Chem. Phys. Lett.* **2000**, *331*, 262.
(7) Gagliardi, L.; Evangelisti, S.; Bernhardsson, A.; Lindh, R.; Roos, B. O. *Int. J. Quantum Chem.* **2000**, *77*, 311.
(8) Bitterereva, M.; Brinck, T.; Ostmark, H. *J. Phys. Chem. A* **2000**, *104*, 11999.
(9) Wang, X.; Tian, A.; Wang, N. B.; Law, C.-K.; Lee, W. K. *Chem. Phys. Lett.* **2001**, *338*, 367.
(10) Kortus, J.; Pederson, M. R.; Richardson, S. L. *Chem. Phys. Lett.* **2001**, *340*, 565.
(11) Tobita, M.; Bartlett, R. J. *J. Phys. Chem. A* **2001**, *105*, 4107.
(12) Wang, X.; Ren, Y.; Shuai, M. B.; Wong, N. B.; Li, W. K.; Tian, A. M. THEOCHEM (*J. Mol. Struct.)* **2001**, *538*, 145.
(13) Ren, Y.; Wang, X.; Wong, N. B.; Tian, A. M.; Ding, F. J.; Zhang, L. F. *Int. J. Quantum Chem.* **2001**, *82*, 34.
(14) Li, Q. S.; Wang, L. J. *J. Phys. Chem. A* **2001**, *105*, 1203.
(15) Gagliardi, L.; Orlandi, G.; Evangelisti, S.; Roos, O. *J. Chem. Phys.* **2001**, *114*, 10733.
(16) Gagliardi, L.; Evangelisti, S.; Barone, V.; Roos, B. O. *Chem. Phys. Lett.* **2000**, *320*, 518.
(17) Gagliardi, L.; Evangelisti, S.; Widmark, P.-O.; Roos, B. O. *Theor. Chem. Acc.* **1997**, *97*, 136.
(18) Korkin, A. A.; Balkova, A.; Bartlett, R. J.; Boyd, R. J.; Schleyer, P. v. R. *J. Phys. Chem.* **1996**, *100*, 5702.
(19) Stront, D. L. *J. Phys. Chem. A* **2002**, *106*, 816.
(20) Vij, A.; Wilson, W. W.; Vij, V.; Tham, F. S.; Sheehy, J. A.; Christie, K. O. *J. Am. Chem. Soc.* **2001**, *123*, 6308.
(21) Nguyen, M. T.; Ha, T.-K. *Chem. Phys. Lett.* **2000**, *317*, 135.
(22) Nguyen, M. T.; Ha, T.-K. *Chem. Phys. Lett.* **2001**, *335*, 311.
(23) Bitterereva, M.; Brinck, T.; Osmark, H. *Chem. Phys. Lett.* **2001**, *340*, 597.
(24) Fau, S.; Bartlett, R. J. *J. Phys. Chem. A* **2001**, *105*, 4096.
(25) Lee, T. J.; Dateo, C. E. *Chem. Phys. Lett.* **2001**, *345*, 295.
(26) Bitterereva, M.; Ostmark, H.; Brink, T. *Chem. Phys. Lett.* **2001**, *347*, 220.
(27) Lee, E. P. F.; Dyke, J. M.; Mok, D. K. W.; Claridge, R. P.; Chau, F. T. *J. Phys. Chem. A* **2001**, *105*, 9533.
(28) Greetham, G. M.; Hanton, M. J.; Ellis, A. M. *Phys. Chem. Chem. Phys.* **1999**, *1*, 2709.
(29) For examples, see Haslett, T. L.; Fedrigo, S.; Bosnick, K.; Moskovits, M.; Duarte, H. A.; Salahub, D. *J. Am. Chem. Soc.* **2000**, *122*, 6039. Mortensen, J. J.; Hansen, L. B.; Hammer, B.; Norskov, J. K. *J. Catal.* **1999**, *182*, 479. Heinemann, C.; Schwarz, J.; Schwarz, H. *J. Phys. Chem.* **1996**, *100*, 6088. Ciullo, G.; Rosi, M.; Sgamelloti, A.; Floriani, C. *Chem. Phys. Lett.* **1991**, *185*, 522. Seigbahn, P. E. M.; Blomberg, M. R. A. *Chem. Phys.* **1984**, *87*, 189. Hidai, M.; Mizobe, Y. *Chem. Rev.* **1995**, *95*, 1115.
(30) Gagliardi, L.; Pyykko, P. *J. Am. Chem. Soc.* **2001**, *123*, 9700.
(31) Gagliardi, L.; Pyykko, P. *J. Phys. Chem. A* **2002**, *106*, 4690.
(32) Burke, L. A.; Butler, R. N.; Stephens, J. C. *J. Chem. Soc., Perkin Trans. 2* **2001**, 1679.
(33) Chang, C.; Patzer, A. B. C.; Sedlmayr, E.; Steinke, T.; Sulzle, D. *Chem. Phys.* **2001**, *271*, 283.
(34) Meloni, G.; Gingerich, K. A. *J. Chem. Phys.* **2000**, *113*,10978.
(35) Nayak, S. K.; Khana, S. N.; Jena, P. *Phys. Rev. B* **1998**, *57*, 3787.
(36) Kandalam, A. K.; Pandey, R.; Blanco, M. A.; Costales, A.; Racio, J. M.; Newsam, J. M. *J. Phys. Chem. B* **2000**, *104*, 4361.
(37) BelBruno, J. J. *Chem. Phys. Lett.* **1999**, *313*, 795.
(38) Andrews, L.; Zhou, M.; Chertihin, G. V.; Bare, W. D. *J. Phys. Chem. A* **2000**, *104*, 1656.
(39) Pelissier, M.; Malrieu, J. P. *J. Mol. Spectrosc.* **1979**, *77*, 322.
(40) Langhoff, S. R.; Bauschlicher, C. W., Jr.; Petersson, L. G. M. *J. Chem. Phys.* **1988**, *89*,7354.
(41) Boo, B. H.; Liu, Z. *J. Phys. Chem. A* **1999**, *103*, 1250.
(42) Gutsev, G. L.; Jena, P.; Bartlett, R. J. *J. Chem. Phys.* **1999**, *110*, 2928.
(43) Chaban, G.; Gordon, M. S. *J. Chem. Phys.* **1997**, *107*, 2160.

(44) Frisch, M. J.; Trucks, G. W.; Schlegel, H. B.; Scuseria, G. E.; Robb, M. A.; Cheeseman, J. R.; Zakrzewski, V. G.; Montgomery, J. A., Jr.; Stratmann, R. E.; Burant, J. C.; Dapprich, S.; Millam, J. M.; Daniels, A. D.; Kudin, K. N.; Strain, M. C.; Farkas, O.; Tomasi, J.; Barone, V.; Cossi, M.; Cammi, R.; Mennucci, B.; Pomelli, C.; Adamo, C.; Clifford, S.; Ochterski, J.; Petersson, G. A.; Ayala, P. Y.; Cui, Q.; Morokuma, K.; Malick, D. K.; Rabuck, A. D.; Raghavachari, K.; Foresman, J. B.; Cioslowski, J.; Ortiz, J. V.; Stefanov, B. B.; Liu, G.; Liashenko, A.; Piskorz, P.; Komaromi, I.; Gomperts, R.; Martin, R. L.; Fox, D. J.; Keith, T.; Al-Laham, M. A.; Peng, C. Y.; Nanayakkara, A.; Gonzalez, C.; Challacombe, M.; Gill, P. M. W.; Johnson, B. G.; Chen, W.; Wong, M. W.; Andres, J. L.; Head-Gordon, M.; Replogle, E. S.; Pople, J. A. *Gaussian 98*; Gaussian, Inc.: Pittsburgh, PA, 1998.

(45) Knowles, P. J.; Hampel, C.; Werner, H. J. *J. Chem. Phys.* **1993**, *99*, 5219.

(46) MOLPRO is a package of ab initio programs written by Werner, H.-J. and Knowles, P. J. with contributions from Almlöf, J.; Amos, R. D.; Berning, A.; Cooper, D. L.; Deegan, M. J. O.; Dobbyn, A. J.; Eckert, F.; Elbert, S. T.; Hampel, C.; Lindh, R.; Lloyd, A. W.; Meyer, W.; Nicklass, A.; Peterson, K.; Pitzer, R.; Stone, A. J.; Taylor, P. R.; Mura, M. E.; Pulay, P.; Schütz, M.; Stoll, H.; and Thorsteinsson, T.

(47) Lee, E. P. F.; Dyke, J. M. *J. Phys. Chem. A* **2000**, *104*, 11810.

(48) Boys, S. F.; Bernardi, F. *Mol. Phys.* **1970**, *19*, 553.

(49) Lee, E.P. F. *Mol. Phys.* **1993**, *78*, 875.

(50) Lauderdale, W. J.; Stanton, J. F.; Bartlett, R. J. *J. Phys. Chem.* **1992**, *96*, 1173.